Journal of Sound and Vibration (1998) **217**(1), 43–74
Article No. sv981744

STATISTICS OF VIBRATION ENERGY FLOW IN RANDOMLY PARAMETERED TRUSSES

C. S. Manohar and S. Adhikari†

Department of Civil Engineering, *Indian Institute of Science*, *Bangalore* 560 012, *India*

(*Received* 22 *May* 1997, *and in final form* 16 *April* 1998)

The problem of determining the ensemble averages of vibration energy flow in harmonically driven trusses with random parameter variations is considered. The mass, elasticity, damping and length of the truss members are modelled as random variables. The uncertainty associated with member lengths result in randomness in truss geometry. Four different linear damping models for truss members, namely, strain rate dependent viscous/hysteretic models and velocity dependent viscous/hysteretic models are considered. The analysis employs random dynamic stiffness matrices and Monte Carlo simulation procedures. A comparison of the ensemble averages of subsystem energies obtained using this approach and those using statistical energy analysis (SEA) formalism is also made. The energy coefficient matrix arising in SEA studies is determined using the direct dynamic stiffness matrix approach. The paper illustrates the relative importance of alternative damping models and alternative sources of system randomness on the behavior of spectra of subsystem vibration energies in a 13-member truss. The uncertainties in randomness in truss geometry and the choice of damping model are shown to significantly affect the energy statistics.

1. INTRODUCTION

Several publications addressing the theoretical foundations of statistical energy analysis (SEA) have appeared over the last decade [1–6]. While these studies have provided valuable insights into the range of applicability of SEA, the determination of variability in vibration energy spectra arising in SEA modelling, on the other hand, has largely remained an open research problem. This issue is of fundamental importance in estimating confidence intervals associated with the averages predicted by SEA. In a recent state of the art review, Fahy [4] identified this class of problems as requiring further research attention and, also, Lyon and DeJong [5], in their recent book on SEA, described the associated problems as being part of a "major piece of unfinished business in SEA . . .". The difficulties associated with this problem can be traced to the following complicating features: (1) The problem of determining energy flow variability requires the determination

† Present address: University of Cambridge, Department of Engineering, Cambridge CB2 1PZ, U.K.

0022–460X/98/410043 + 32 $30.00/0

of the probability distribution of the vibration energy spectra. This problem is analytically not easily tractable. Rules of transformation of random variables are difficult to apply and no discernible patterns in mathematical expressions for energy levels exist which would enable the application of limit theorems of probability. (2) The energy spectra, viewed as random processes evolving in the frequency parameter, are non-stationary in nature. This is especially true in regions of low modal overlap. Thus, the assumption of ergodicity of these spectra is inadmissible. Consequently, decisions based on a limited number of samples (often a single sample), using frequency band averages, are difficult to validate. (3) To conduct experiments on a stochastic ensemble of vibrating systems, one should be able to produce in laboratories such ensembles with specified statistical properties, which, again, is not easy. (4) No feasible statistical models for system parameters which are based on field observations exist and, consequently, knowledge is lacking in postulating appropriate stochastic models for system property variations.

In view of these difficulties, several researchers have performed numerical experiments on simple structural configurations with hypothesized uncertainty models. The analysis here is carried out within the frameworks of Monte Carlo simulations and frequency domain vibration analysis techniques such as those using system Green's function (receptances) or dynamic stiffness matrices. Such studies have enabled identification of factors influencing variability in spectra of vibration energies. The study reported in this paper belongs to studies of this genre. We begin by briefly describing some of the earlier related investigations.

Davies and Wahab [7] considered the statistics of coupling loss factors across the intermediate support of a two-span continuous beam with one of the spans subjected to rain on the roof type of excitations. The ratio of the two spans was modelled as a random variable with uniform probability distribution function. The same system under the action of point harmonic forcing was considered by Davies and Khandoker [8] and results were presented on the statistics of cross power receptance function. These studies illustrated the importance of the subsystem modal overlap factor, defined as the ratio of average modal bandwidth to the average spacing of natural frequencies, as a parameter influencing the response variability. As may be expected, the variability was found to be higher for lower modal overlap factors. Fahy and Mohammed [9] considered systems of spring coupled beams, plates and rods and noted the non-Gaussian nature of the energy flow characteristics at low modal overlap factors and concluded that the confidence limits cannot be estimated using the mean and standard deviation alone.

Keane and Manohar [10] and Manohar and Keane [11, 12] considered the energy flows in spring coupled beam and rod systems and investigated the effects of the following factors on the probabilistic characteristics of power receptance functions: choice of subsystem types, damping models, strength of system randomness, type of excitation and types of system randomness. The study considered both Gaussian and non-Gaussian random variable/random process models for the mass, stiffness and geometrical properties of the rod/beam elements and surveyed the statistics of the power receptance functions. It was noted that

these receptance functions are non-stationary random processes with the non-stationarity arising due to occurrence of resonances and the variation of mode shapes at the point of driving, coupling and measurement with changes in the driving frequency. However, it was noticed in most, but not all cases, that with increases in driving frequency, the receptance functions tended to be stochastically stationary. This indicated that a frequency exists beyond which the receptance can be expected to reach a stochastic "steady" state and consequently, beyond this frequency, a simplified description of system behavior through procedures such as SEA can be expected to be possible. Analogous to the definition of a modal overlap factor, a modal statistical overlap factor was defined as the ratio of standard deviation of the natural frequency to the average spacing of the natural frequencies [12]. This factor enabled identification of frequency beyond which the statistics of the spectra cease to "oscillate". It was concluded that since both these overlap factors could vary with frequency, precise knowledge of their behavior was a precursor to the successful application of SEA methods. Furthermore, the same study has also demonstrated that the probability distribution of the response power spectra can be very well approximated by either gamma or lognormal probability distributions. These considerations have further been examined by Keane [13] in the context of vibration energy flow in a pair of line coupled random membranes.

The study by Rebillard and Guyader [14] considers a system of a pair of rectangular plates coupled along edges and executing harmonic flexural and in-plane vibrations. The connection angle between the two plates is modelled as a Gaussian random variable. The in-plane and flexural motions are uncoupled only if the connection angle is zero. The study has shown that when the nominal angle of connection is small, the uncertainty in system response is higher than when the angle is large. Mace [15] and Wester and Mace [16] adopt dynamical analysis based on wave propagation theory and they combine this with simulation procedures to investigate the ensemble averages of energy flow in simple built-up structures.

2. PRESENT STUDY

Most of the studies mentioned in the previous section focus their attention on relatively small sized problems with a number of coupled subsystems, most often being only two. Thus, in these studies, the question of randomness in system geometry does not assume significant importance. In large sized structures, however, the randomness in specifying nodal locations would be another source of system randomness. Besides, the influence of different models for damping and the manner in which the damping is spatially distributed also has not been studied extensively. These issues are addressed in the present study. Specifically, this paper considers the vibration energy flow in a truss structure with reference to the following aspects: (1) Development of the stochastic dynamic stiffness matrix approach combined with the Monte Carlo simulation technique to study ensemble statistics of vibration energy distribution in trusses due to point harmonic excitations. (2) Study of the influence of different sources of system randomness

on behavior ensemble averages; for this purpose, the mass, elasticity, damping and lengths of the truss members are considered to be a set of random variables; the randomness in lengths of individual members introduces randomness in the truss geometry. (3) Comparison between the results of ensemble averages using stochastic dynamic stiffness matrix analysis and the results from frequency band averaging using SEA calculations. (4) Use of dynamic stiffness matrices in evaluation of the energy coefficient matrix arising in the SEA calculation; the questions of close coupling and far coupling between subsystems are also considered in these calculations. (5) Investigation into the probability distribution of the spectrum of vibration energies.

3. A SINGLE TRUSS ELEMENT

With reference to Figure 1, the equation of motion of an axially vibrating rod element can be written as

$$\frac{\partial}{\partial x}\left\{AE\frac{\partial Y}{\partial x}+\left[\eta_1+\frac{\eta_2}{\omega}\right]AE\frac{\partial^2 Y}{\partial x\partial t}\right\}=m\frac{\partial^2 Y}{\partial t^2}+\left\{c_1+\frac{c_2}{\omega}\right\}\frac{\partial Y}{\partial t}-F\delta(x-x_0)\exp[\mathrm{i}\omega t]. \tag{1}$$

Here AE = axial stiffness, m = mass per unit length, η_1 = strain rate dependent viscous damping coefficient, η_2 = strain rate dependent hysteretic damping coefficient, c_1 = velocity dependent viscous damping coefficient, c_2 = velocity dependent hysteretic damping coefficient, F = magnitude of the harmonic concentrated force, x_0 = distance at which the force is acting and $\delta(x-x_0)$ represents the Dirac delta function centered at $x=x_0$. In the presence of element harmonic forces and nodal displacements, the displacement within the rod element can be taken to be given by

$$Y(x,t)=y(x)\exp[\mathrm{i}\omega t]. \tag{2}$$

Consequently, the field equation reduces to

$$\frac{\mathrm{d}^2 y}{\mathrm{d}x^2}+b^2 y=\frac{-F\delta(x-x_0)}{AE[1+\mathrm{i}\eta_1\omega+\mathrm{i}\eta_2]}, \tag{3}$$

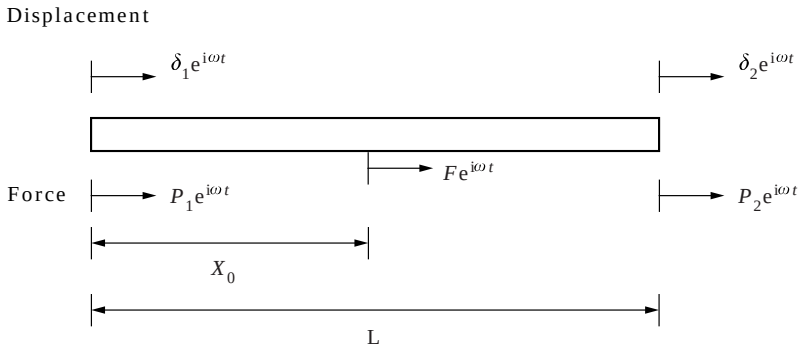

Figure 1. Axially vibrating truss element.

where

$$b^2 = \frac{m\omega^2 - \mathrm{i}c_1\omega - \mathrm{i}c_2}{AE[1 + \mathrm{i}\eta_1\omega + \mathrm{i}\eta_2]}. \tag{4}$$

It is clear that b is complex valued. The displacement field with $y(0) = \delta_1$ and $y(L) = \delta_2$ is given by

$$Y(x, t) = \left[\delta_1 \cos bx + \frac{\delta_2 - \delta_1 \cos bL}{\sin bL} \sin bx + \frac{F \sin b(L - x_0)}{AE(1 + \mathrm{i}\eta_1\omega + \mathrm{i}\eta_2)} \frac{\sin bx}{\sin bL}\right]$$

$$\times \exp[\mathrm{i}\omega t] \quad \text{for } x \leqslant x_0,$$

$$Y(x, t) = \left[\delta_1 \cos bx + \frac{\delta_2 - \delta_1 \cos bL}{\sin bL} \sin bx + \frac{F \sin b(L - x_0)}{AE(1 + \mathrm{i}\eta_1\omega + \mathrm{i}\eta_2)} \frac{\sin bx}{\sin bL}\right.$$

$$\left. - \frac{F \sin b(x - x_0)}{AE(1 + \mathrm{i}\eta_1\omega + \mathrm{i}\eta_2)}\right] \exp[\mathrm{i}\omega t] \quad \text{for } x \geqslant x_0. \tag{5}$$

The quantities δ_1 and δ_2 are in general complex valued.

3.1. ENERGETICS OF A TRUSS ELEMENT

The expressions for the total strain energy $\bar{U}(\omega)$, total kinetic energy $\bar{T}(\omega)$ and the total energy dissipated $\bar{D}(\omega)$ in the rod averaged over the time interval $(0, 2\pi/\omega)$ are given by

$$\bar{U}(\omega) = \left[\frac{\omega}{2\pi}\right] \frac{1}{2} \int_0^{2\pi/\omega} \int_0^L AE \left[\text{Real} \left\{\frac{\partial Y}{\partial x}\right\}\right]^2 \mathrm{d}x\, \mathrm{d}t, \tag{6}$$

$$\bar{T}(\omega) = \left[\frac{\omega}{2\pi}\right] \frac{1}{2} \int_0^{2\pi/\omega} \int_0^L m \left[\text{Real} \left\{\frac{\partial Y}{\partial t}\right\}\right]^2 \mathrm{d}x\, \mathrm{d}t, \tag{7}$$

$$\bar{D}_{c_1}(\omega) = \left[\frac{\omega}{2\pi}\right] \int_0^{2\pi/\omega} \int_0^L c_1 \left[\text{Real} \left\{\frac{\partial Y}{\partial t}\right\}\right]^2 \mathrm{d}x\, \mathrm{d}t,$$

$$\bar{D}_{c_2}(\omega) = \left[\frac{\omega}{2\pi}\right] \int_0^{2\pi/\omega} \int_0^L \frac{c_2}{\omega} \left[\text{Real} \left\{\frac{\partial Y}{\partial t}\right\}\right]^2 \mathrm{d}x\, \mathrm{d}t$$

$$\bar{D}_{\eta_1}(\omega) = -\left[\frac{\omega}{2\pi}\right] \int_0^{2\pi/\omega} \int_0^L \eta_1 AE \left[\text{Real} \left\{\frac{\partial Y}{\partial t}\right\} \text{Real} \left\{\frac{\partial^3 Y}{\partial x^2\, \partial t}\right\}\right] \mathrm{d}x\, \mathrm{d}t,$$

$$\bar{D}_{c_1}(\omega) = -\left[\frac{\omega}{2\pi}\right] \int_0^{2\pi/\omega} \int_0^L \frac{\eta_2 AE}{\omega} \left[\text{Real} \left\{\frac{\partial Y}{\partial t}\right\} \text{Real} \left\{\frac{\partial^3 Y}{\partial x^2\, \partial t}\right\}\right] \mathrm{d}x\, dt,$$

$$\bar{D}(\omega) = \bar{D}_{c_1}(\omega) + \bar{D}_{c_2}(\omega) + \bar{D}_{\eta_1}(\omega) + \bar{D}_{\eta_2}(\omega). \tag{8}$$

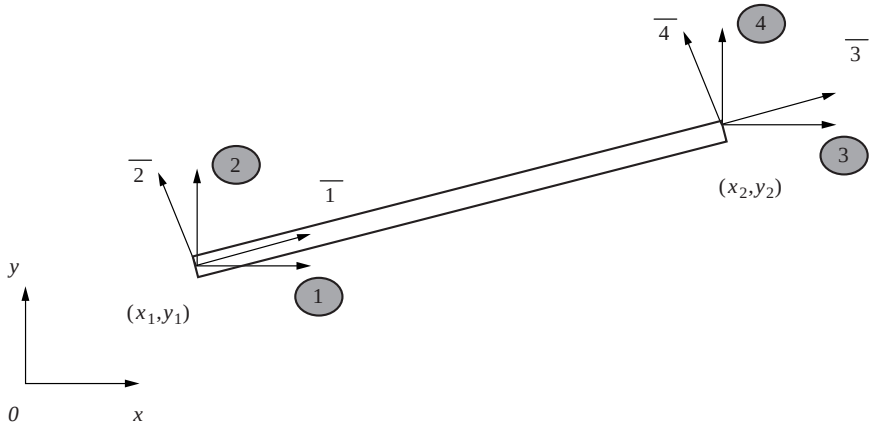

Figure 2. Local and global co-ordinates.

Here $\bar{D}_{c_1}(\omega)$, $\bar{D}_{c_2}(\omega)$, $\bar{D}_{\eta_1}(\omega)$ and $\bar{D}_{\eta_2}(\omega)$ correspond to the contributions to $\bar{D}(\omega)$ made by damping terms involving c_1, c_2, η_1 and η_2 respectively. In our studies, the integrals appearing in equations (6–8) were evaluated symbolically using MAPLE V. The primary response variable in this study is the total vibration energy given by

$$E(\omega) = \bar{U}(\omega) + \bar{T}(\omega). \tag{9}$$

A useful feature which emerges from the study of the expressions for energy spectra is that the energy dissipated can be expressed as a fraction of the kinetic energy as follows

$$\frac{\bar{D}_{c_1}(\omega)}{\bar{T}(\omega)} = 2\,\frac{c_1}{m}, \qquad \frac{\bar{D}_{c_2}(\omega)}{\bar{T}(\omega)} = 2\,\frac{c_2}{\omega m},$$

$$\frac{\bar{D}_{\eta_1}(\omega)}{\bar{T}(\omega)} = 2\,\frac{(\alpha^2-\beta^2)AE\eta_1}{m}, \qquad \frac{\bar{D}_{\eta_2}(\omega)}{\bar{T}(\omega)} = 2\,\frac{(\alpha^2-\beta^2)AE\eta_2}{\omega m}. \tag{10}$$

Here $\alpha = \text{Real}\,[b]$ and $\beta = \text{Imag}\,[b]$. These expressions enable the computation of dissipation energies as fractions of kinetic energies.

3.2. DYNAMIC STIFFNESS MATRIX AND EQUIVALENT NODAL FORCE VECTOR

The dynamic stiffness matrix for an undamped axially vibrating rod is readily available in the literature [17]. For a damped axially vibrating rod, the dynamic stiffness matrix is symmetric and complex valued. With reference to Figure 2, the

member dynamic stiffness coefficients in global co-ordinates can be shown to be given by

$$D^e_{G_{1,1}}(\omega) = \frac{AEb\cos(bL)(x_2^2 - 2x_2x_1 + x_1^2)}{L^2\sin(bL)},$$

$$D^e_{G_{1,2}}(\omega) = \frac{AEb\cos(bL)(x_2y_2 - x_2y_1 - x_1y_2 + x_1y_1)}{L^2\sin(bL)},$$

$$D^e_{G_{1,3}}(\omega) = -\frac{AEb(x_2^2 - 2x_2x_1 + x_1^2)}{L^2\sin(bL)},$$

$$D^e_{G_{1,4}}(\omega) = -\frac{AEb(x_2y_2 - x_2y_1 - x_1y_2 + x_1y_1)}{L^2\sin(bL)},$$

$$D^e_{G_{2,2}}(\omega) = \frac{AEb\cos(bL)(y_2^2 - 2y_2y_1 + y_1^2)}{L^2\sin(bL)},$$

$$D^e_{G_{2,3}}(\omega) = -\frac{AEb(x_2y_2 - x_2y_1 - x_1y_2 + x_1y_1)}{L^2\sin(bL)},$$

$$D^e_{G_{2,4}}(\omega) = -\frac{AEb(y_2^2 - 2y_2y_1 + y_1^2)}{L^2\sin(bL)},$$

$$D^e_{G_{3,3}}(\omega) = \frac{AEb\cos(bL)(x_2^2 - 2x_2x_1 + x_1^2)}{L^2\sin(bL)},$$

$$D^e_{G_{3,4}}(\omega) = \frac{AEb\cos(bL)(x_2y_2 - x_2y_1 - x_1y_2 + x_1y_1)}{L^2\sin(bL)},$$

$$D^e_{G_{4,4}}(\omega) = \frac{AEb\cos(bL)(y_2^2 - 2y_2y_1 + y_1^2)}{L^2\sin(bL)}, \tag{11}$$

where L is the length of the member. Notice that only the elements of the upper triangular matrix are listed above. The presence of force within the element results in the equivalent nodal forces. Thus, corresponding to the concentrated force $F\exp[i\omega t]$ acting at $x = x_0$, see Figure 1, the amplitude of the equivalent nodal force in global co-ordinates can be shown to be given by

$$f^e_G = -\begin{bmatrix} \dfrac{(x_2 - x_1)F(-\cot(bL)\sin(bx_0) + \cos(bx_0))}{L} \\ \dfrac{(y_2 - y_1)F(-\cot(bL)\sin(bx_0) + \cos(bx_0))}{L} \\ \dfrac{(x_2 - x_1)F\,\mathrm{cosec}(bL)\sin(bx_0)}{\mathrm{L}} \\ \dfrac{(y_2 - y_1)F\,\mathrm{cosec}(bL)\sin(bx_0)}{\mathrm{L}} \end{bmatrix}. \tag{12}$$

It may be noted that the presence of damping makes the dynamic stiffness coefficients and equivalent nodal forces to be complex valued.

3.3. MODAL DAMPING, BANDWIDTH AND OVERLAP FACTOR

Although the present study does not employ normal mode expansion for response analysis, still it is of interest to consider the nature of modal equations which would result from equation (1). In general, the equation for the frequency response function corresponding to the nth generalized co-ordinate can be given by

$$H_n(\omega, \omega_n) = \frac{1}{-\omega^2 + i2\xi_n\omega_n\omega + \omega_n^2}, \tag{13}$$

where $\xi_n =$ the coefficient of damping of the nth mode and $\omega_n = n$th natural frequency. Furthermore, the quantity $B_n = 2\xi_n\omega_n$ is the modal bandwidth. The damping coefficient and modal bandwidth can be shown to be given respectively by

$$\xi_n = \frac{c_2}{2m\omega_n\omega} + \frac{c_1}{2m\omega_n} + \frac{\eta_2}{2}\frac{\omega_n}{\omega} + \eta_1\omega_n,$$

$$B_n = \frac{c_2}{m\omega} + \frac{c_1}{m} + \eta_2\frac{\omega_n^2}{\omega} + \eta_1\omega_n^2. \tag{14}$$

If a resonant condition $\omega = \omega_n$ is assumed to prevail, then, it follows

$$\xi_n = \frac{c_2}{2m\omega^2} + \frac{c_1}{2m\omega} + \frac{\eta_2}{2} + \frac{\eta_1\omega}{2},$$

$$B_n = \frac{c_2}{m\omega} + \frac{c_1}{m} + \eta_2\omega + \eta_1\omega^2. \tag{15}$$

Thus, B_n and ξ_n appear as linear combinations of terms involving ω^{-2}, ω^{-1}, ω^0, ω^1 and ω^2. It must be noted that, since, for a truss element the subsystem natural frequencies are uniformly spaced, the modal overlap factor becomes linearly dependent on the modal bandwidth. The behavior of modal damping coefficient, bandwidth and overlap factor as a function of ω is thus strongly influenced by the chosen modal for the damping and it will be demonstrated later that this variation has a major influence on the behavior of the energy spectra.

4. TRUSS EXAMPLE: DETERMINISTIC ANALYSIS

As a prelude to the statistical analysis of vibration energy flow in an ensemble of trusses, the energy flow calculations for the case of a deterministic truss are first considered. The approach adopted is based on the inversion of the global dynamic stiffness matrix of the structure. This provides an elegant framework to treat alternative damping models and also provides uniformly accurate results at all values of the driving frequency. It may be noted that the use of the dynamic stiffness matrix in vibration energy flow calculation in skeletal structures has been discussed earlier by Langley [18]. An alternative approach based on series representation of subsystem Green's functions is also available [3, 19]. For the purpose of illustration, the truss shown in Figure 3 has been selected. All the members of the truss are taken to have an axial stiffness $AE = 23{\cdot}75 \times 10^6$ N and

mass per unit length $m = 0{\cdot}882$ kg/m. The truss is driven by a vertical point harmonic excitation at node 5 and we are interested in determining the total vibration energy over a cycle, i.e., $E(\omega)$, in all the truss members as a function of ω. The global dynamic stiffness matrix is obtained by following the usual rules of structural matrix assembling as is used in the static finite element analysis. The inversion of this matrix leads to the nodal displacements which in turn enable the computation of various energy quantities using equations (6)–(8). In the numerical work, five models for damping are considered: (a) all members have identical velocity dependent viscous damping with $c_1 = 60{\cdot}96$ Ns/m^2; (b) all members have identical velocity dependent hysteretic damping with $c_2 = 42{\cdot}132 \times 10^3$ N/m^2; (c) all members have identical strain rate dependent viscous damping with $\eta_1 = 1{\cdot}468 \times 10^{-4}$ s; (d) all members have identical strain rate dependent hysteretic damping with $\eta_2 = 0{\cdot}1015$; (e) all top chord members (2, 3, 4) have identical strain rate dependent viscous damping with $\eta_1 = 1{\cdot}468 \times 10^{-4}$ s, all bottom chord members (6, 7, 8) have identical strain rate dependent hysteretic damping with $\eta_2 = 0{\cdot}1015$, all vertical members (1, 10, 12, 5) have identical velocity dependent viscous damping with $c_1 = 60{\cdot}96$ Ns/m^2 and all diagonal elements (9, 11, 13) have identical velocity dependent hysteretic damping with $c_2 = 42{\cdot}132 \times 10^3$ N/m^2.

The value of c_1 in model (a) is selected on the basis that the damping coefficient in the first mode is 1·5%. For this value of damping, the dissipated energy as a fraction of $\bar{T}(\omega)$ is computed using equation (10). The values of the other damping model parameters, c_2, η_1 and η_2 in models (b–d) are then selected such that in all these models, at the first natural frequency, the same fraction of $\bar{T}(\omega)$ gets dissipated as in model (a). Figure 4 shows $E(\omega)$ for the top chord members, 2, 3 and 4, for the above damping models. It has been verified that in all these cases the power input is numerically equal to the sum of energy dissipated in all the truss members; this serves as a check on the correctness of the calculations made. The behavior of $E(\omega)$ for large frequencies is seen to be strongly governed by the choice of damping model. From equation (15) it follows that for the first four damping types listed above, (a–d), the bandwidth parameter, B_n, varies as ω^0, ω^{-1}, ω^2 and ω, respectively. It can be expected that the behavior of $E(\omega)$ at large frequencies

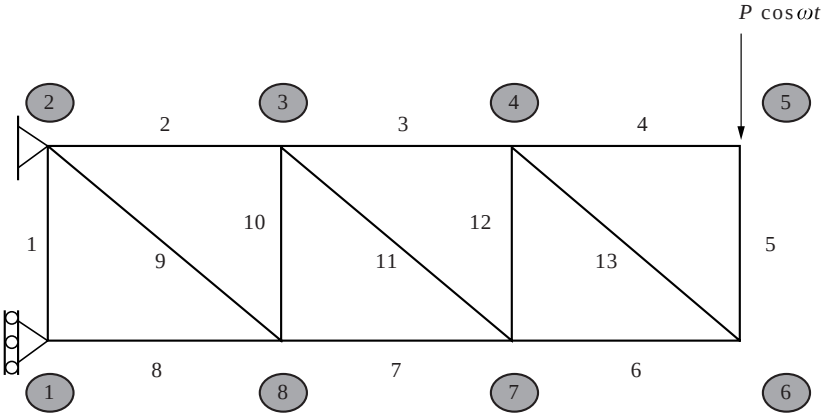

Figure 3. The example truss considered; for all members: $AE = 23{\cdot}75 \times 10^6$ N; $m = 0{\cdot}882$ kg/m.

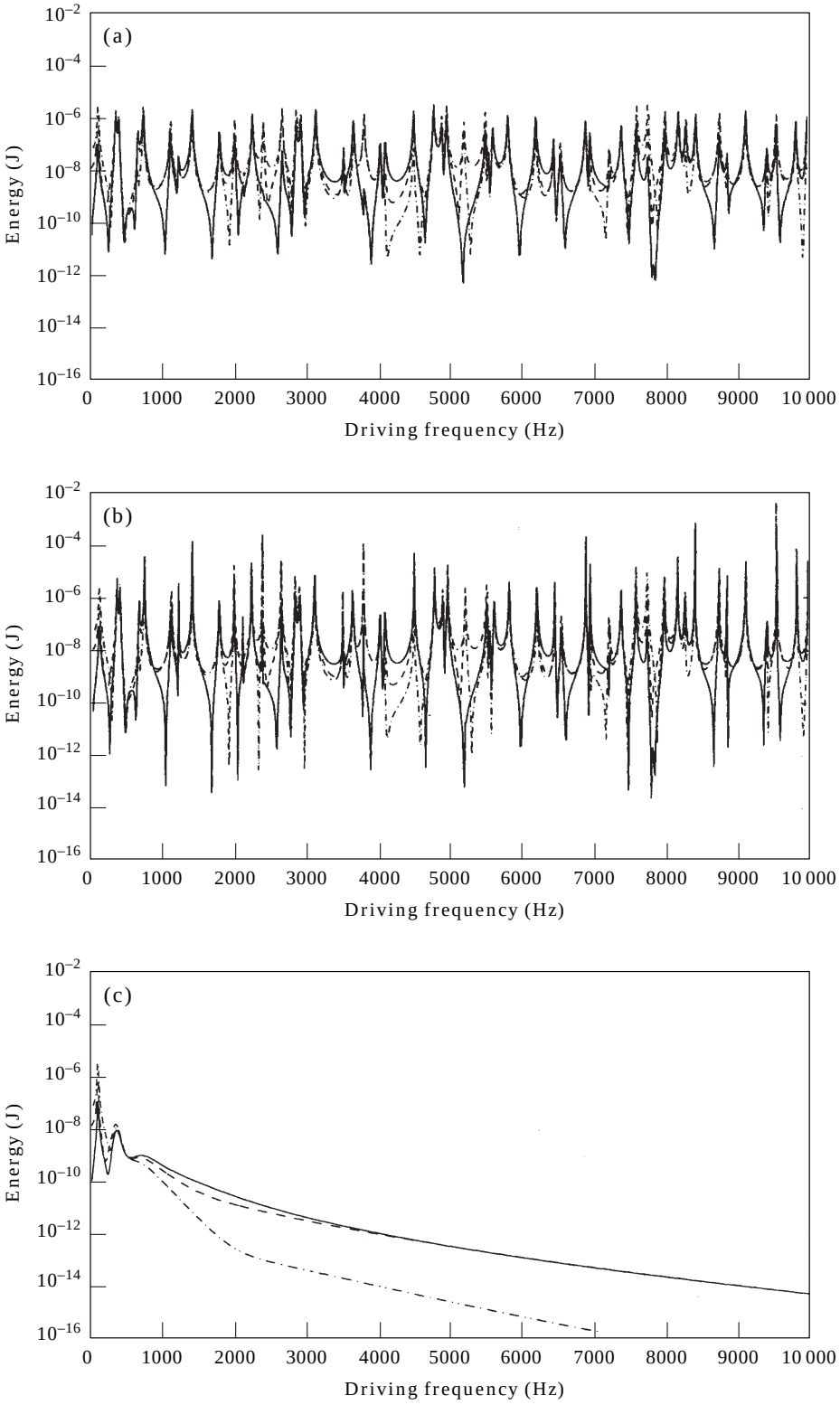

Figure 4(a–c). *Caption opposite*.

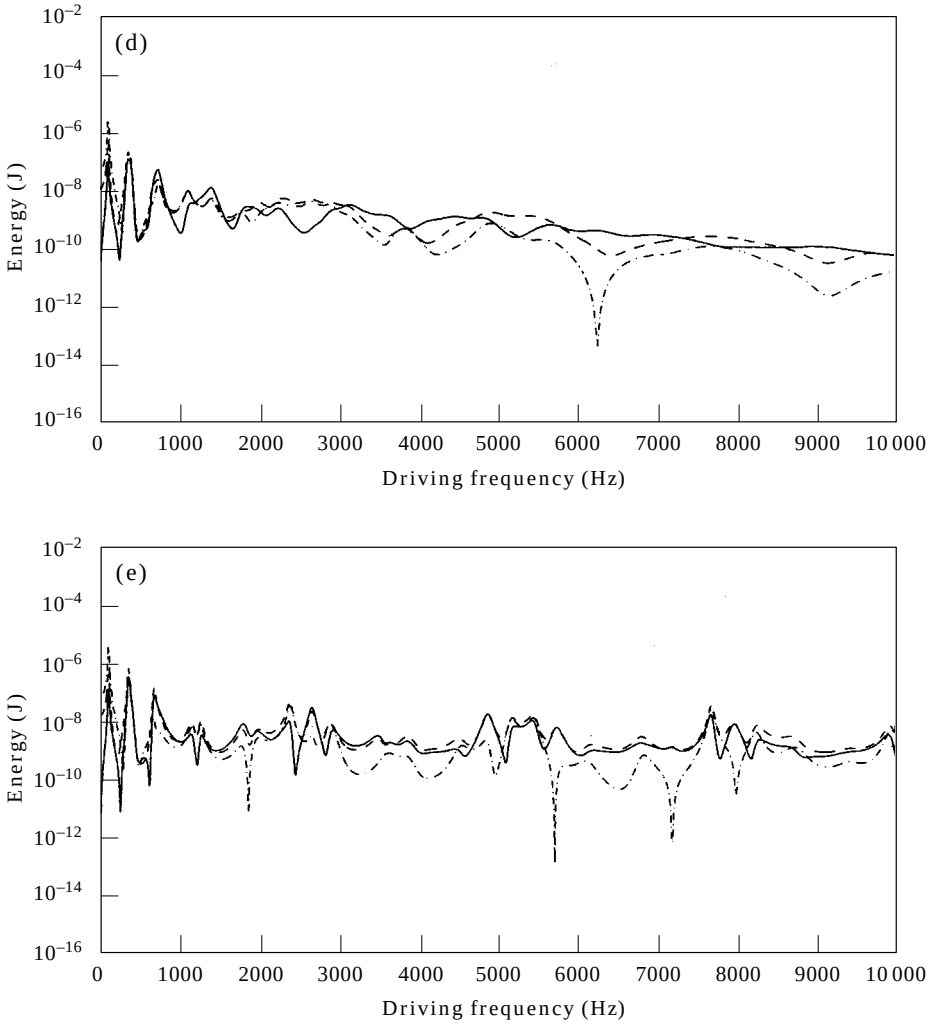

Figure 4. Energy spectra for top chord of the nominal truss; - . - . -, Member 2; - - -, member 3; —, member 4. (a) Damping type (a); (b) damping type (b); (c) damping type (c); (d) damping type (d); (e) damping type (e).

is *smoother* for systems having larger B_n. The results of Figure 4 endorse this expectation, in which the fluctuations in $E(\omega)$ is observed to be the largest for case (b) (Figure 4(b)), and is the smoothest for case (c) (Figure 4(c)). In case (e), different truss members have different damping models and the results presented serve to illustrate the flexibility of dynamic stiffness matrix method in handling different damping models.

5. TRUSS EXAMPLE: STOCHASTIC ANALYSIS

The first step in the analysis of vibrating systems with parameter uncertainties is the choice of the probabilistic models for uncertainties. In the traditional SEA,

the subsystem natural frequencies are taken to be a set of mutually independent random variables distributed uniformly in the frequency band of interest. In this study, however, the physical parameters of the truss are modelled as being random. These models could be in terms of random fields or, at a much simpler level, in terms of a set of random variables. For problems of the first category, the random fields need to be discretized into an equivalent set of random variables. Recently, the present authors have considered a dynamic stiffness matrix of general beam elements with spatially random inhomogenieties and have proposed a discretization scheme involving frequency dependent shape functions [20]. In the present study, however, our attention is restricted to random variable models and it is assumed that, for every truss member, the elastic stiffness parameter AE, mass per unit length m, damping parameters c_1, c_2, η_1 and η_2 form a set of mutually independent random variables. Additionally, we are interested in treating radomness in truss geometry. The following two options are considered to achieve this: (1) model the length of individual truss members as a set of independent random variables; consequently, the nodal co-ordinates, (x_i, y_i), become a set of mutually dependent random variables; (2) model the nodal co-ordinates (x_i, y_i) as a set of independent random variables; consequently, the member lengths become a set of mutually independent random variables.

It is felt that the first option is more realistic, since, in practice, the lengths of truss members are more likely to be the primary quantities than the nodal co-ordinates, and, therefore, this option is adopted in our study. Attention is again focused on the specific 13-member truss example considered in the previous section. Let the vector of random variables $[AE_i, m_i, c_{1i}, c_{2i}, \eta_{1i}, \eta_{2i}, L_i]^{\mathrm{T}}$, (T = matrix transpose), represent the uncertainty associated with the ith truss element. All these vectors, that is, with $i = 1, \ldots, 13$, can now be assembled in a matrix $\mathbf{U}$ with the elements taken to be given by

$$\mathbf{U}_{ij} = \bar{U}_{ij}[1 + \epsilon_{ij} W_{ij}]; \qquad i = 1, \ldots, 13, \qquad j = 1, \ldots, 7, \tag{16}$$

where $\varepsilon_{ij} > 0$ is a deterministic constant and $\bar{U}_{ij}$ is the vector of nominal values of the system parameter. W_{ij} are a set of random variables which are taken in this study to be mutually independent, identical and distributed uniformly in $[-1, 1]$. The parameter ε_{ij}, thus, denotes the strength of the randomness associated with the jth element of the random variable vector associated with member i. Thus, for example, ε_{27} denotes the strength of randomness in the length of member 2. Referring to equations (11), it becomes apparent that the member dynamic stiffness coefficients in global co-ordinates are now a set of complex valued random processes evolving in the parameter ω. Upon assembling the element dynamic stiffness matrix, following the usual rules of structural matrix assembling, one gets the structure dynamic stiffness matrix. This matrix can be shown to be random, symmetric and complex valued. The evaluation of energy spectra $E(\omega)$ for the truss members requires the inversion of this random matrix. This problem is analytically not easily tractable, especially when elements of the random matrix are non-Gaussian in nature [21], and, hence, in this study, the Monte Carlo simulation procedures are adopted to solve the problem.

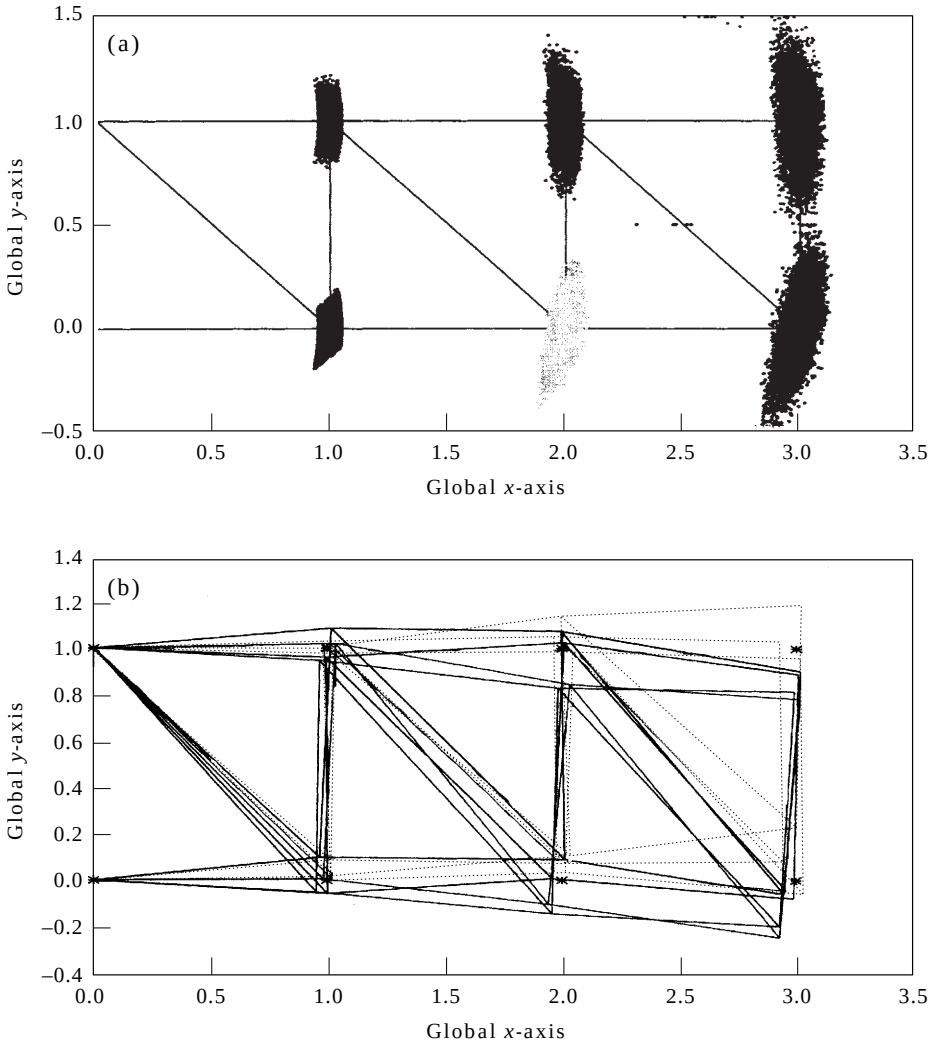

Figure 5. (a) Scatter of nodal co-ordinates of truss with random geometry; —, nominal truss. (b) Sample realizations of truss with random geometry; *, nominal location of the nodes.

As has been already noted, as a consequence of taking member lengths to be random variables, the nodal co-ordinates (x_i, y_i) become a set of mutally correlated random variables. This in turn, imparts randomness to the geometry of the truss (see Figures 5(a) and (b)). The determination of the nodal co-ordinates (x_i, y_i) $(i = 1, 8)$, requires the solution of the following set of non-linear algebraic equations:

$$x_1 = 0; \qquad y_1 = 0; \qquad x_2 = 0; \qquad y_2 = L_1;$$

$$y_8 = \frac{1}{2y_2}\{L_8^2 + y_2^2 - L_9^2\}; \qquad x_8 = \sqrt{(L_8^2 - y_8^2)};$$

$$L_{10}^2 - \{x_2 - x_8 + \sqrt{(L_2^2 - (y_3 - y_2)^2)}\}^2 - (y_3 - y_8)^2 = 0;$$

$$x_3 = x_2 + \sqrt{(L_2^2 - (y_3 - y_2)^2)};$$

$$L_{11}^2 - \{x_8 - x_3 + \sqrt{(L_7^2 - (y_7 - y_8)^2)}\}^2 - (y_7 - y_3)^2 = 0;$$

$$x_7 = x_8 + \sqrt{(L_7^2 - (y_7 - y_8)^2)};$$

$$L_{12}^2 - \{x_3 - x_7 + \sqrt{(L_3^2 - (y_4 - y_3)^2)}\}^2 - (y_4 - y_7)^2 = 0;$$

$$x_4 = x_3 + \sqrt{(L_3^2 - (y_4 - y_3)^2)};$$

$$L_6^2 - \{x_4 - x_7 + \sqrt{(L_{13}^2 - (y_6 - y_4)^2)}\}^2 - (y_6 - y_7)^2 = 0;$$

$$x_6 = x_4 + \sqrt{(L_{13}^2 - (y_6 - y_4)^2)};$$

$$L_5^2 - \{x_4 - x_6 + \sqrt{(L_4^2 - (y_5 - y_4)^2)}\}^2 - (y_5 - y_6)^2 = 0;$$

$$x_5 = x_4 + \sqrt{(L_4^2 - (y_5 - y_4)^2)}. \tag{17}$$

These equations have been listed in the order in which they are solved in the numerical algorithm. A careful inspection of these equations reveals that these equations can be solved sequentially such that, at any given step, only one non-linear equation needs to be handled. Figure 5(b) shows a few sample realizations of the truss geometries in which the randomness parameters, ε_{17}, $(i = 1, \ldots, 13)$, associated with the member lengths, are taken to be 0·05.

To evaluate the relative importance of different sources of system randomness, the energy spectra $E_i(\omega)$, $(i = 1, \ldots, 13)$, have been evaluated with: (A) randomness in all the elements of U_{ij} with $\varepsilon_{ij} = 0{\cdot}05$; (B) randomness in all the elements of U_{ij} $\varepsilon_{ij} = 0{\cdot}05$, except the randomness associated with the member lengths; and (C) randomness in member lengths alone with no randomness in other quantities with $\varepsilon_{i7} = 0{\cdot}05$ and 0·01. Numerical results on ensemble statistics of $E(\omega)$ using the digital simulations of 500 samples are shown in Figure 6. Results are presented on moments of $E(\omega)$ for the member 3, for the five damping models listed in section 4 and for the randomness model A. The choice of damping model is observed to largely control the behavior of ensemble statistics as a function of driving frequency. For damping models, for which the bandwidth increases with driving frequency (models c and d), the ensemble statistics become smooth (Figures 6(c) and (d)). On the other hand, for damping models (a) and (b), for which the bandwidth does not increase with frequency, the ensemble averages remain "oscillatory", thereby indicating that the response is governed by individual resonances (Figures 6(a) and 6(b)). For the combined damping model, Figure 6(e), the behavior, as may be expected, consists of no systematic "oscillatory" or "smooth" trends. A measure of dispersion in the response is defined as the difference in 95% and 50% probability points. Figure 7 shows this measure as a function of ω for member 3 for the damping models (a) to (e). For damping model (c), in which the modal bandwidth parameter B_n varies as ω^2, the dispersion measure reduces monotonically with increases in frequency and remains lower than the results from all the other models. On the other hand, for damping model (b) for which B_n varies as ω^{-1}, the dispersion measure is higher than the results of the rest of the models. The relative importance of different sources of

randomness is depicted in Figures 8(a) and (b), in which the ratio of dispersion measures for randomness models A, B and C are shown for members 3 and 5 for damping model (a). The dispersion measure for systems with randomness in geometry is seen to be significantly higher than that due to other sources of uncertainties. Thus, it is concluded that the choice of damping model and randomness in truss geometry play important roles in deciding the qualitative and quantitative behavior of the response statistics.

6. TRUSS EXAMPLE: STATISTICAL ENERGY ANALYSIS

The approach outlined in the previous section is an "exact" approach to determine the spectra of average total energy distribution in the truss structure. This is true from the point of view of both the dynamical analysis of sample problems (since the dynamic stiffness matrix method is used) and from the point of view of statistical analysis (since the Monte Carlo simulations are used). On the other hand, the traditional SEA, which also aims at predicting the spectra of average total energy distribution, introduces approximations in both dynamics and statistical aspects of response calculations [1, 5, 12, 22]. Thus, it is of interest to compare the results obtained in the previous section with calculations performed within the SEA framework. Such comparisons are again illustrated through the truss example shown in Figure 3.

6.1. ENERGY COEFFICIENTS

A major step in the SEA of built-up structures is the identification of the matrix of coupling loss factors [5, 2, 18]. There has been considerable interest in the use of finite element analysis (FEA) in estimating the SEA coupling loss factors [23–26]. These methods basically simulate on a computer the power injection method of finding coupling loss factors experimentally [27, 28]. The analysis can be carried out in two possible ways: (I) Here attention is focused on the built up structure in its entirety and energy in all the members is found by injecting power into individual subsystems by turn; this is equivalent to conducting the experiment on the complete structure and, hence, the coupling between all the constituent members is completely accounted for. (II) Here, the structure is considered to be an assembly of several subsystems and each subsystem is studied divorced from the main structure; this is equivalent to conducting experiments on a set of substructures and synthesizing the results of built up structure from the results of the parts.

In this study, the above two methods are employed to estimate the coupling loss factors within the framework of the dynamic stiffness matrix approach. The merits of this approach, in relation to the FEA based approach, are: (a) since no modal expansion is used, errors due to modal truncation is avoided; (b) the method is uniformly accurate over the entire frequency range of interest; and (c) different damping models and damping magnitudes can be assigned to different members.

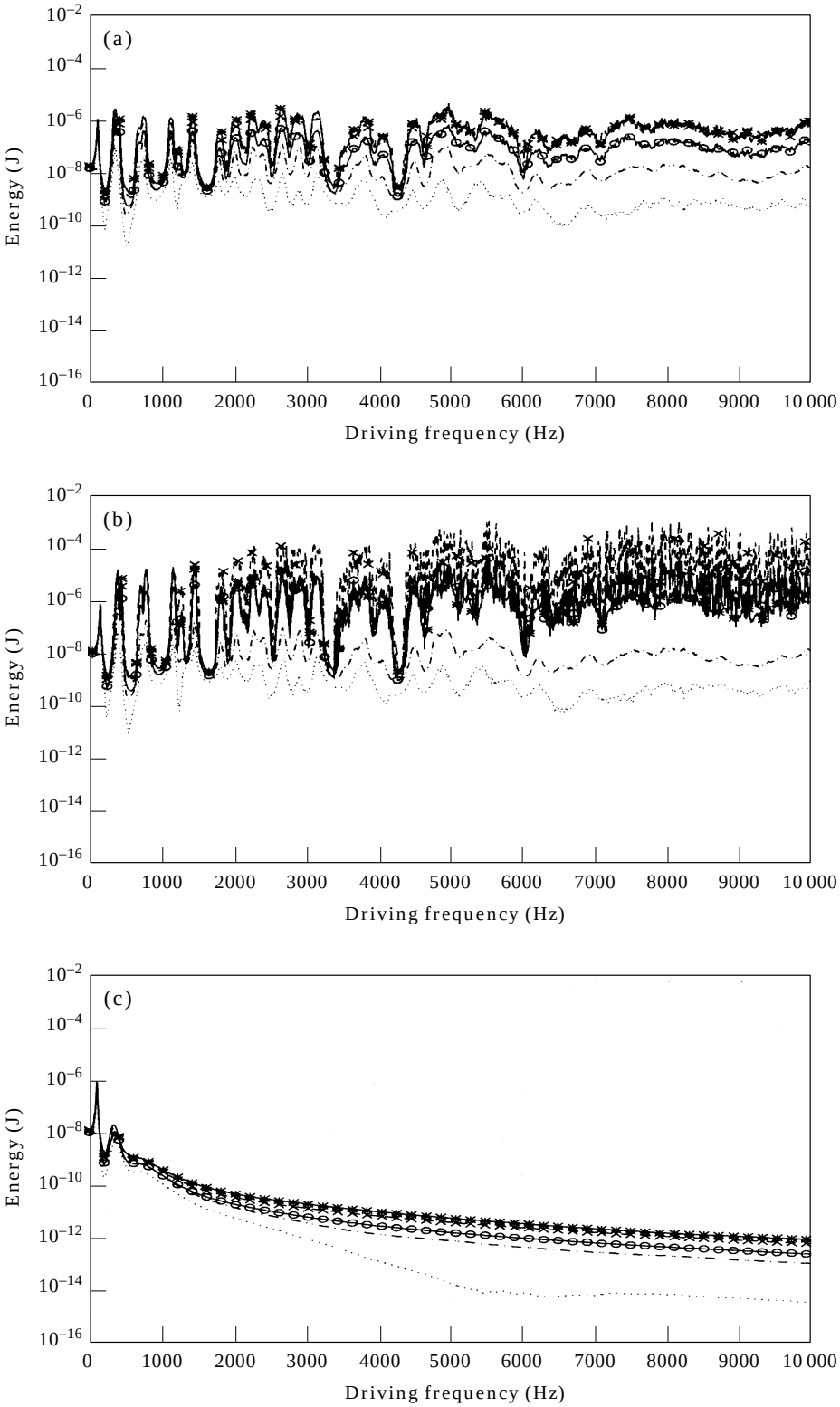

Figure 6(a–c). *Caption opposite*.

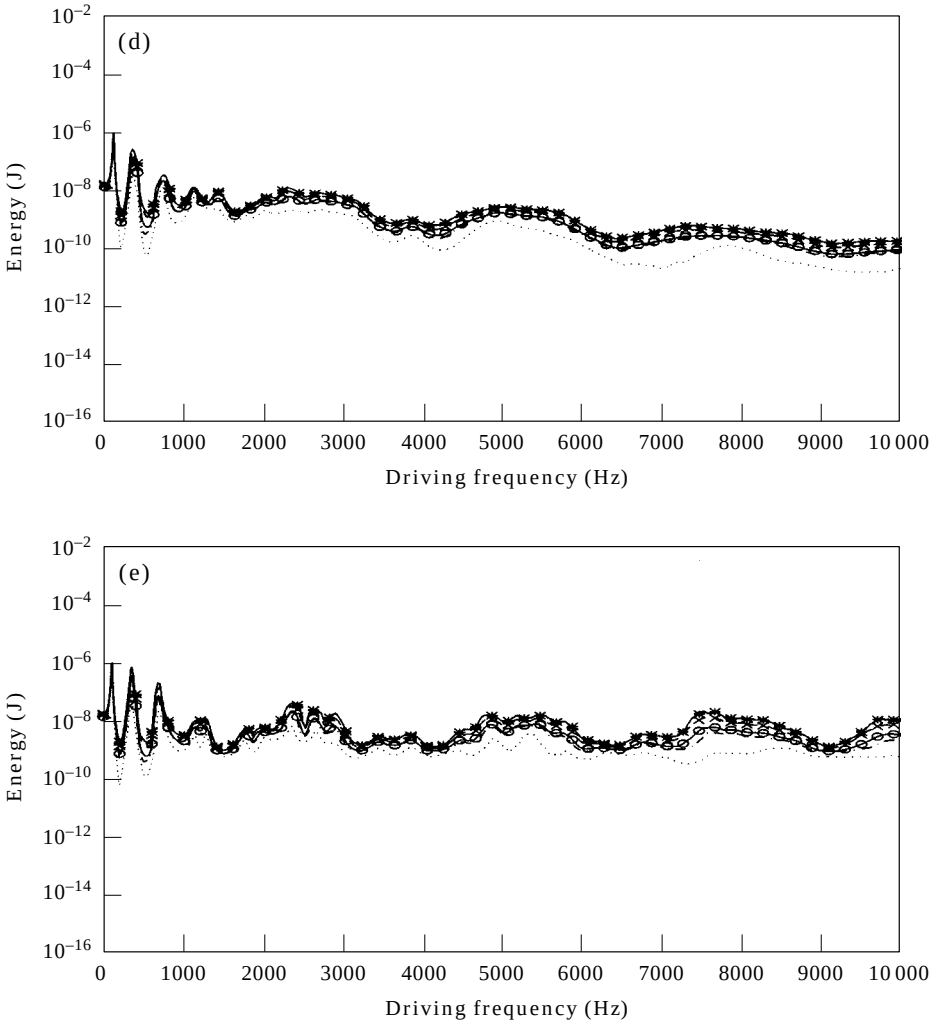

Figure 6. Ensemble averages of $E(\omega)$ for member 3; sample size = 500; uncertainty model A; . . . . , 5 percentage points; - . - . -, 50 percentage points; -*-*-, 95 percentage points; -○-○-, mean; - × - × -, mean + standard deviation. (a) Damping type (a); (b) damping type (b); (c) damping type (c); (d) damping type (d); (e) damping type (e).

6.1.1. *Method I*

In this method the truss structure shown in Figure 3 is divided into 13 SEA subsystems with each truss member representing one subsystem. Furthermore, all the subsystems are taken to be coupled with each other. We begin by applying a point harmonic force of magnitude f_k at a randomly chosen point x_k within the ith member and the total vibration energy given by equation $E_{ij}^{(k)}(\omega)$ is computed for all the truss members $j = 1, \ldots, 13$. Also, the power input $\Pi_i^{(k)}(\omega)$ is computed using the formula

$$\Pi_i^{(k)}(\omega) = \tfrac{1}{2}\,\text{Real}\,[f_k V_{x_k}^*(\omega)], \tag{18}$$

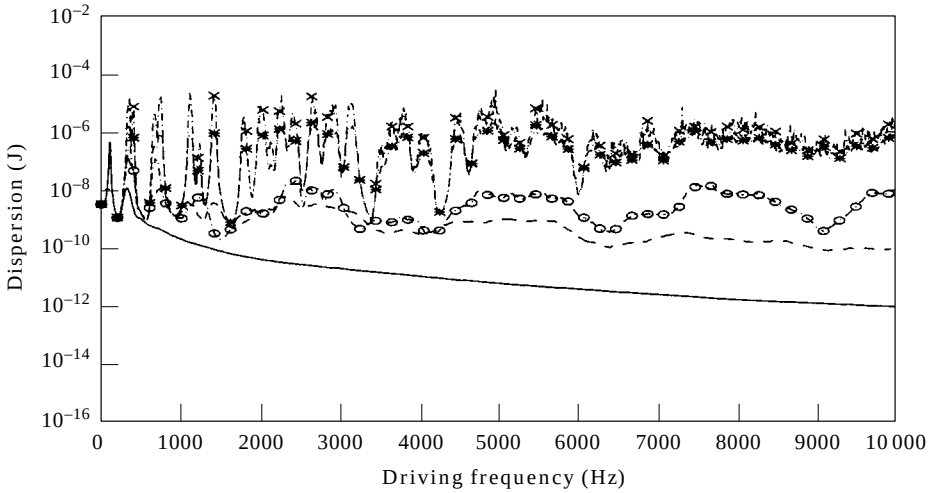

Figure 7. Measure of dispersion in $E(\omega)$ for member 3; -*-*-, damping type (a); - × - × -, damping type (b); —, damping type (c); - - - , damping type (d); -○-○-, damping type (e).

where $V_{x_k}(\omega) =$ amplitude of vellocity at x_k and $* =$ conjugation. These calculations are repeated for five randomly chosen points of harmonic load application. The estimates of $E_{ij}(\omega)$, the energy in the jth subsystem due to the power input at the ith subsystem, and $\Pi_i^{(k)}(\omega)$, the power input to the ith subsystem are evaluated using the expressions

$$E_{ij}(\omega) = \frac{1}{5}\sum_{k=1}^{5} E_{ij}^{(k)}(\omega), \qquad \Pi_i(\omega) = \frac{1}{5}\sum_{k=1}^{5} \Pi_i^{(k)}(\omega). \tag{19}$$

These calculations are repeated for all the truss members by taking $i = 1, \ldots, 13$. It is assumed that $E_{ij}(\omega)$ and $\Pi_i(\omega)$ are linearly related through the relation

$$[C_{ij}(\omega)][E_{ij}(\omega)] = \text{Diag}\,[\Pi_i]. \tag{20}$$

These equations represent a set of simultaneous equations for the coefficients $[C_{ij}(\omega)]$, $(i, j = 1, \ldots, 13)$. Thus, $C_{ij}(\omega)$ are determined and these can further be used to determine the energy distribution in the truss structure when it is loaded by loads other than those considered in evaluating these coefficients. It may be remarked here that the symmetry of the matrix of coupling loss factors implied by the reciprocity relations [5] is not assumed here; also, it must be noted that the C-matrix is fully populated thereby implying that the "far" coupling effects are taken into account.

6.1.2. *Method II*

In this method the truss is again divided into 13 subsystems but the coupling paths are assumed to exist only amongst "near" coupled subsystems (see Figure 9). Thus, the coupling between members removed from each other by a joint is ignored. Under this assumption, the C-matrix is no longer fully populated and has the following form:

$$C = \begin{bmatrix}
C_{1,1} & C_{1,2} & 0 & 0 & 0 & 0 & 0 & C_{1,8} & C_{1,9} & 0 & 0 & 0 & 0 \\
C_{2,1} & C_{2,2} & C_{2,3} & 0 & 0 & 0 & 0 & 0 & C_{2,9} & C_{2,10} & C_{2,11} & 0 & 0 \\
0 & C_{3,2} & C_{3,3} & C_{3,4} & 0 & 0 & 0 & 0 & 0 & C_{3,10} & C_{3,11} & C_{3,12} & C_{3,13} \\
0 & 0 & C_{4,3} & C_{4,4} & C_{4,5} & 0 & 0 & 0 & 0 & 0 & 0 & C_{4,12} & C_{4,13} \\
0 & 0 & 0 & C_{5,4} & C_{5,5} & C_{5,6} & 0 & 0 & 0 & 0 & 0 & 0 & C_{5,13} \\
0 & 0 & 0 & 0 & C_{6,5} & C_{6,6} & C_{6,7} & 0 & 0 & 0 & C_{6,11} & C_{6,12} & C_{6,13} \\
0 & 0 & 0 & 0 & 0 & C_{7,6} & C_{7,7} & C_{7,8} & C_{7,9} & C_{7,10} & C_{7,11} & C_{7,12} & 0 \\
C_{8,1} & 0 & 0 & 0 & 0 & 0 & C_{8,7} & C_{8,8} & C_{8,9} & C_{8,10} & 0 & 0 & 0 \\
C_{9,1} & C_{9,2} & 0 & 0 & 0 & 0 & C_{9,7} & C_{9,8} & C_{9,9} & C_{9,10} & 0 & 0 & 0 \\
0 & C_{10,2} & C_{10,3} & 0 & 0 & 0 & C_{10,7} & C_{10,8} & C_{10,9} & C_{10,10} & C_{10,11} & 0 & 0 \\
0 & C_{11,2} & C_{11,3} & 0 & 0 & C_{11,6} & C_{11,7} & 0 & 0 & C_{11,10} & C_{11,11} & C_{11,12} & 0 \\
0 & 0 & C_{12,3} & C_{12,4} & 0 & C_{12,6} & C_{12,7} & 0 & 0 & 0 & C_{12,11} & C_{12,12} & C_{12,13} \\
0 & 0 & C_{13,3} & C_{13,4} & C_{13,5} & C_{13,6} & 0 & 0 & 0 & 0 & 0 & C_{13,12} & C_{13,13}
\end{bmatrix}. \quad (21)$$

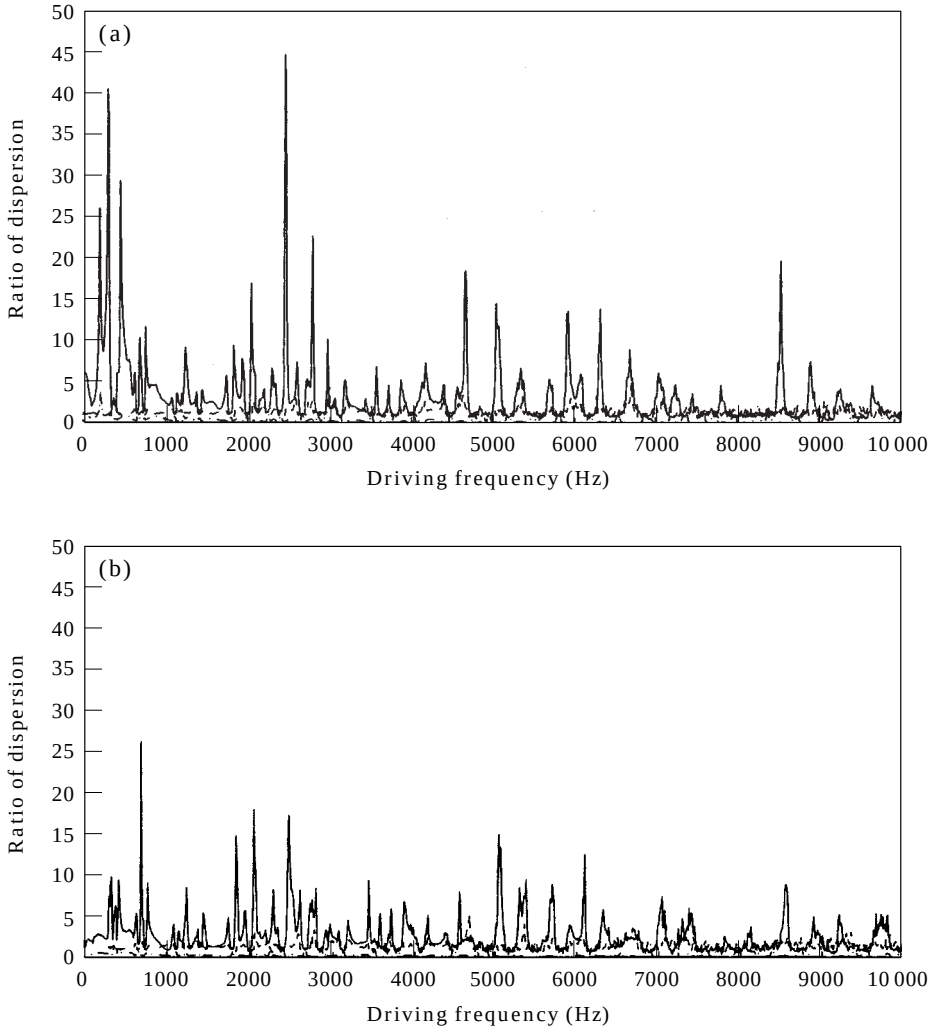

Figure 8. Ratio of dispersion measures for different uncertainty models; damping model (a). (a) Member 3; (b) member 5; —, case C (with $\varepsilon_{i7}=0{\cdot}05$)/case B; - . - . - , case C (with $\varepsilon_{i7}=0{\cdot}01$)/case B; - - - , case A/case C (with $\varepsilon_{i7}=0{\cdot}05$).

A non-zero coefficient C_{ij} in this matrix indicates the existence of a possible *direct* coupling path between the subsystems i and j. To determine these coefficients, the same procedure as described in the previous section is followed but with a difference: the calculations are now performed on a set of substructures. Thus, to determine the quantities $C_{2,2}$, $C_{2,3}$, $C_{2,10}$, $C_{2,11}$, $C_{3,3}$, $C_{3,2}$, $C_{3,11}$, $C_{3,10}$, $C_{10,10}$, $C_{10,2}$, $C_{10,3}$, $C_{10,11}$, $C_{11,2}$, $C_{11,3}$, $C_{11,10}$ and $C_{11,11}$ in the above matrix (see joint 3 in Figure 3), the substructure shown in Figure 10 is considered. A four-member SEA model for this sub-problem is made, as shown in Figure 11. This reduced problem is analyzed again by using the procedure described in the preceding section. Similarly, the remaining quantities of the C-matrix are evaluated by considering SEA models for substructures obtained by isolating members at each of the truss joints.

6.2. ENERGY FLOW CALCULATIONS AND FREQUENCY BAND AVERAGES

Having determined the C-matrix, the problem of determining the energy distribution in the truss when it is driven by a point harmonic excitation is now considered (Figure 3). The power input $\Pi_5(\omega)$ is computed using

$$\Pi_5(\omega) = \tfrac{1}{2}\,\text{Real}\,[PV^*_{y_5}(\omega)], \tag{22}$$

where P = amplitude of the harmonic forcing and $V_{y_5}(\omega)$ = amplitude of velocity at node 5 in the y direction. The energy levels $E_i(\omega)$, $(i = 1, \ldots, 13)$ are determined using

$$\{E(\omega)\} = [C(\omega)]^{-1}\{\Pi\}. \tag{23}$$

Here Π denotes the vector of power input with $\Pi_5(\omega)$ as given by equation (22) and $\Pi_i(\omega) = 0$ for all $i \neq 5$. Numerical work has been carried out for the damping models listed in section 4 and using the two methods of finding $C(\omega)$ described in the previous section. Figures 12 and 13 show the spectra of $E(\omega)$ for members 5 and 3 for the damping model (a). These spectra are now averaged over frequency bands, as is done in the traditional SEA. The 1/3 octave bands with center frequencies of 20, 31·5, 50, 80, 125, 200, 315, 500, 800, 1250, 2000, 5000 and 8000 Hz are selected [5]. This way of averaging amounts to assuming that the spectra consist of segments of random processes which are ergodic within each of the frequency bands considered. The frequency band averages of $E(\omega)$ obtained using methods I and II, are compared with the ensemble statistics in Figures 14 and 15. The ensemble averages correspond to the randomness model A (see section 5). It can be observed that the ensemble mean and frequency average using method I compare reasonably well with each other, especially for driving frequencies beyond 1 kHz, for all the five damping models studied. This lends credence to the computation of the C-matrix using the approach described in section 6.1.1. On the other hand, the results of method II tend to overestimate the mean energy especially for member 3 which is away from the point of driving. This feature arises due to the effect of indirect coupling between near and far subsystems, which method II does not take cognizance of.

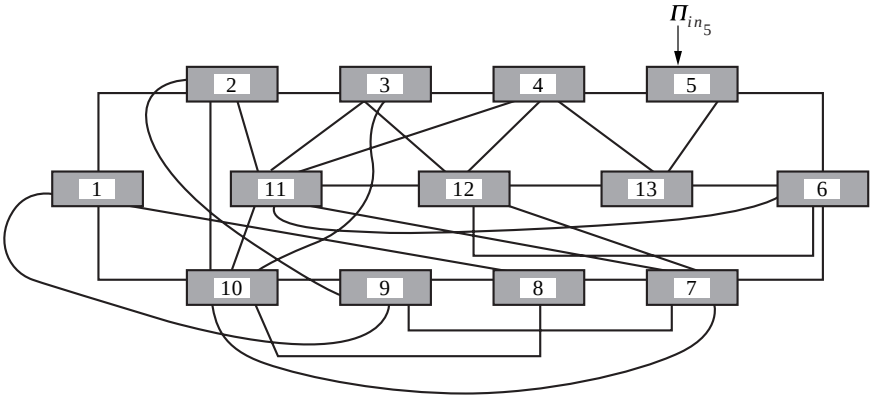

Figure 9. SEA model for the truss example.

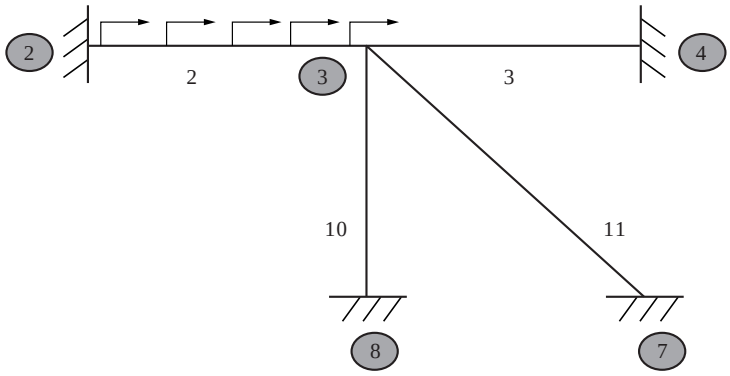

Figure 10. Substructure for computation of the C-matrix.

7. TRUSS EXAMPLE: PROBABILITY DISTRIBUTIONS

The relationship between the random variables U_{ij} describing the system randomness and the spectra of energy is highly non-linear with no clearly discernible patterns. Consequently, determining the probability distribution $E(\omega)$ by rules of transformation of random variables or by invoking any of the limit theorems of probability is difficult. In view of this, it is of interest to investigate if the digitally simulated data on $E(\omega)$ can be described by empirical distributions [12]. Given that $E(\omega) > 0$, the usefulness of fitting exponential, Rayleigh, gamma and lognormal distributions to the simulated data has been investigated. The usefulness of Gaussian distribution with non-zero mean in describing the data was also considered. The parameter estimation capabilities of MATLAB statistics toolbox was employed in this investigation. The range of system parameter variations surveyed included: damping models (types a–e, see section 4), sources of randomness (types A and B, see section 5) and driving frequency (central frequencies of 1/3 octave bands up to 8 kHz). The probability distribution function of $E(\omega)$ for members 5 (close to the point of driving) and 3 (away from the point of driving) were studied. A limited amount of results are shown in Figures 16–18. In each of these figures, the probability distribution of $E(\omega)$, estimated using 5000 samples (marked in the caption as *simulation results*), is shown together with the empirically fitted probability distribution function (marked in the caption as

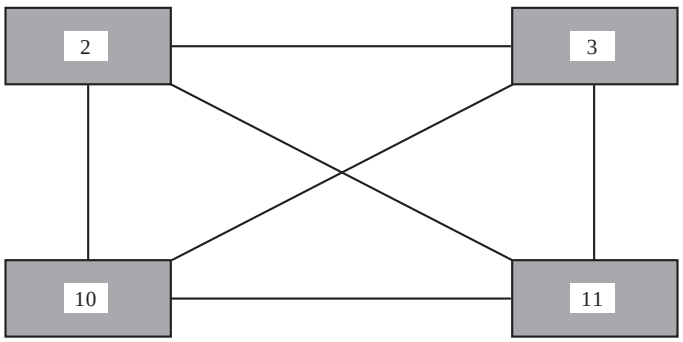

Figure 11. SEA model for the substructure.

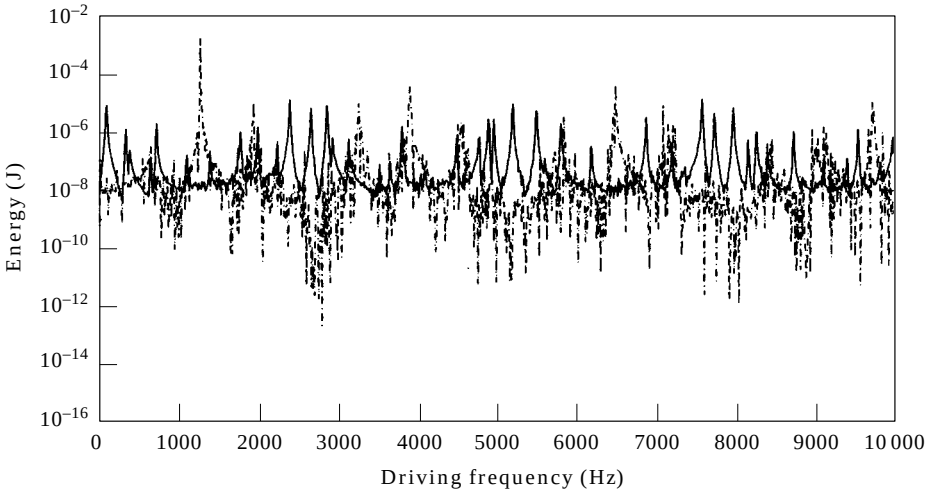

Figure 12. Energy spectra for member 5 before frequency band averaging computed using SEA methods; damping model (a); —, method I; - . - . - , method II.

empirical results). The following were the observations made: (1) lognormal distribution was observed to fit the data better than the other models considered; the goodness of the fit was examined using the Kolmogorov–Smirnov test and in most (but not all) of the cases, it was observed that at 5% significance level, the data could be taken as being lognormal distributed; the cases in which the data did not pass the test includes the cases shown in Figures 16(b), 16(c) and 18(b); (2) the effect of randomness in geometry of the truss was to produce probability distributions which were highly non-Gaussian and had long upper tails, especially in frequency ranges above about 200 Hz and (3) in frequency ranges below about 200 Hz, the data could be well described by Gaussian, gamma or lognormal distributions.

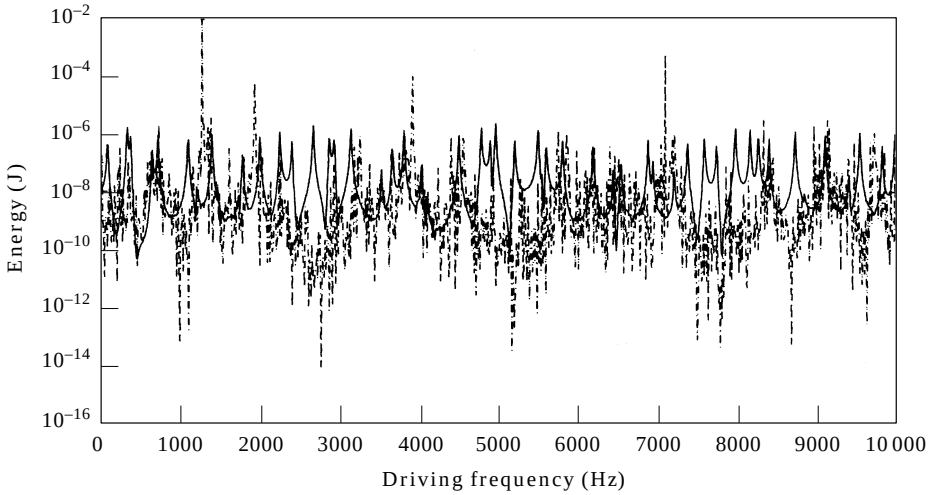

Figure 13. Energy spectra for member 3 before frequency band averaging computed using SEA methods; damping model (a); —, method I; - . - . - , method II.

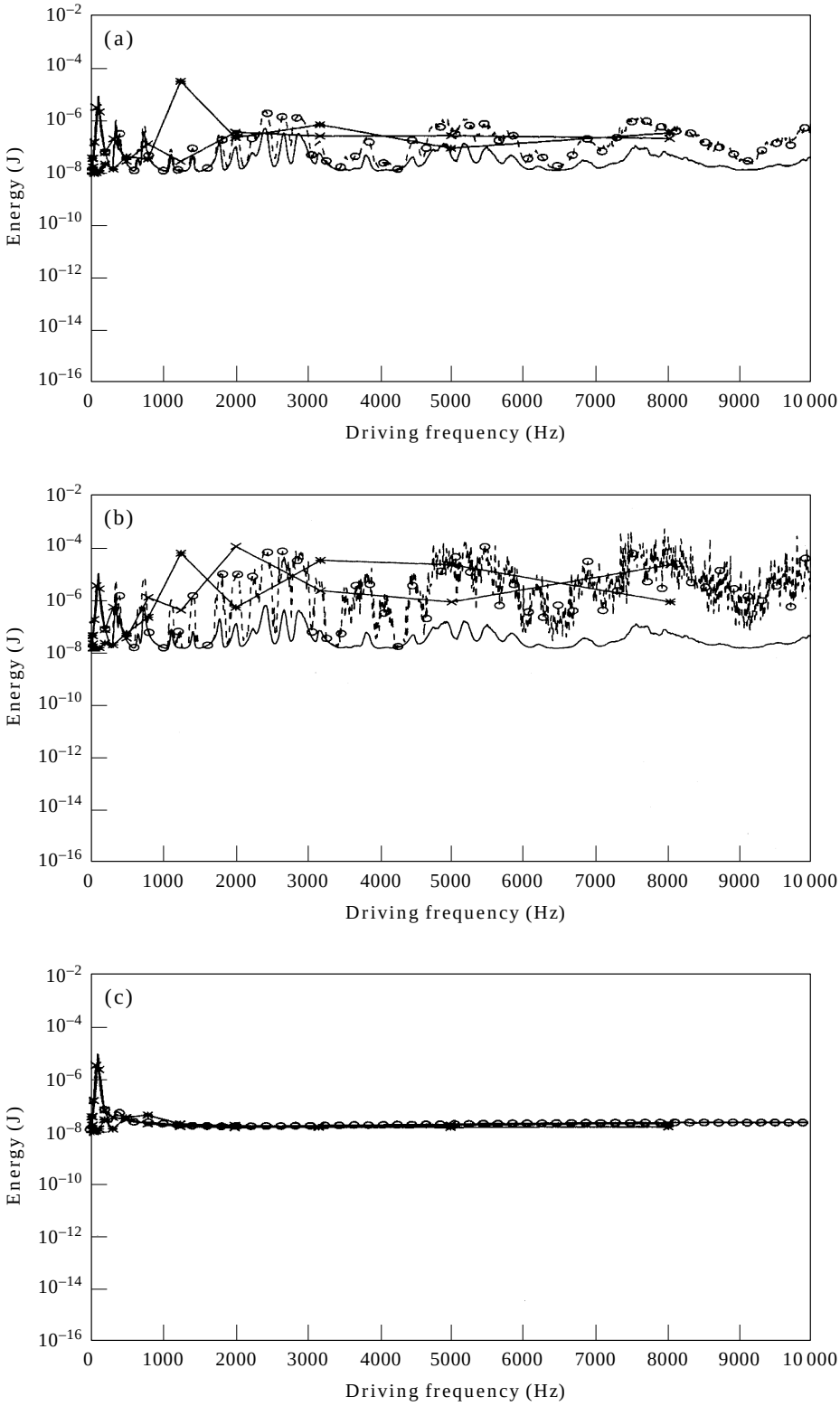
(a)
(b)
(c)
Energy (J)
10^{-2}
10^{-4}
10^{-6}
10^{-8}
10^{-10}
10^{-12}
10^{-14}
10^{-16}
0 1000 2000 3000 4000 5000 6000 7000 8000 9000 10 000
Driving frequency (Hz)

Figure 14(a–c)

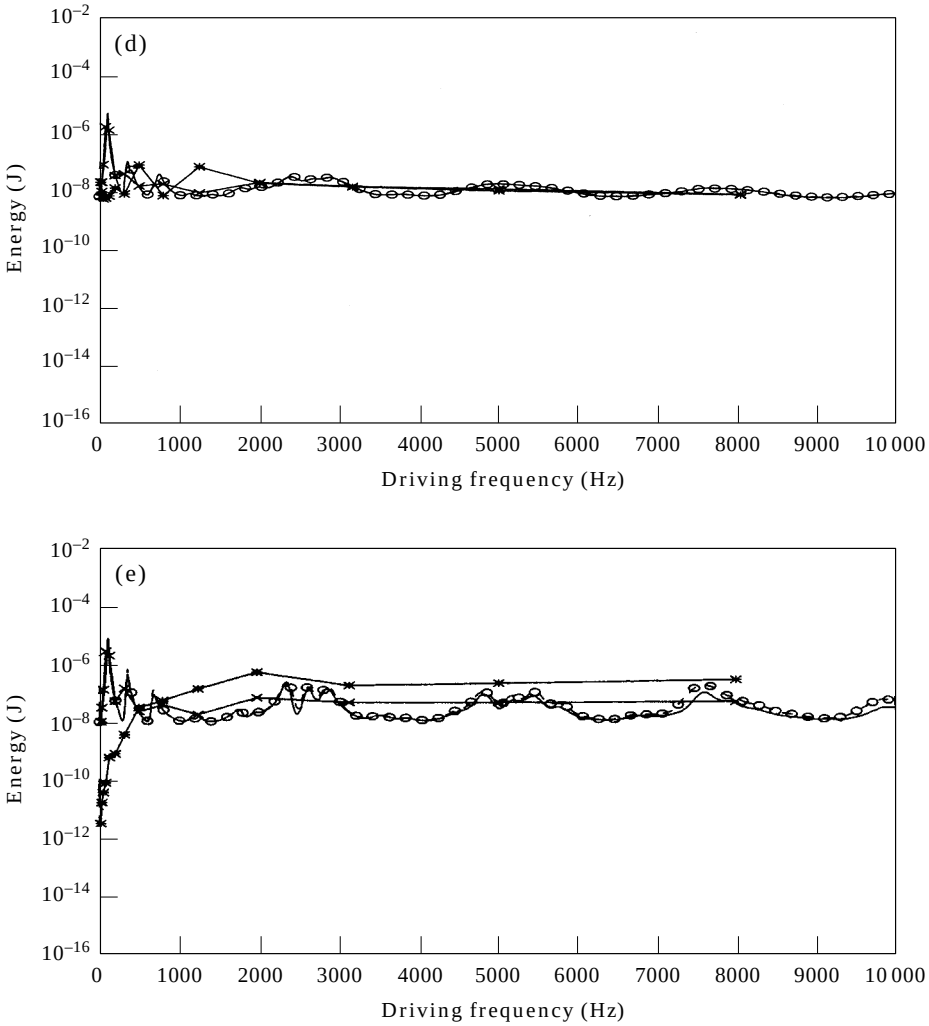

Figure 14. Comparison of ensemble averages and SEA results for member 5; -○-○-, ensemble mean; —, 50 percentage point; -×- × -, SEA: method I; -*-*-, SEA: method II. (a) Damping type (a); (b) damping type (b); (c) damping type (c); (d) damping type (d); (e) damping type (e).

Thus, it may be observed that knowledge of the mean and standard deviation of the energy spectra, in conjunction with the assumption that the spectra are lognormal distributed, enables the estimation of 5% and 95% probability points. An attempt was also made to fit lognormal distributions to the single realization of energy spectra obtained using the SEA approach (section 6) using the frequency band mean and standard deviation. This required the assumption that the spectra consist of segments of random processes which are ergodic not only in the mean, but also in standard deviations over the 1/3 octave frequency bands. The results obtained, however, were highly distorted and did not compare well with the distributions estimated using ensemble averaging. Further work is clearly needed

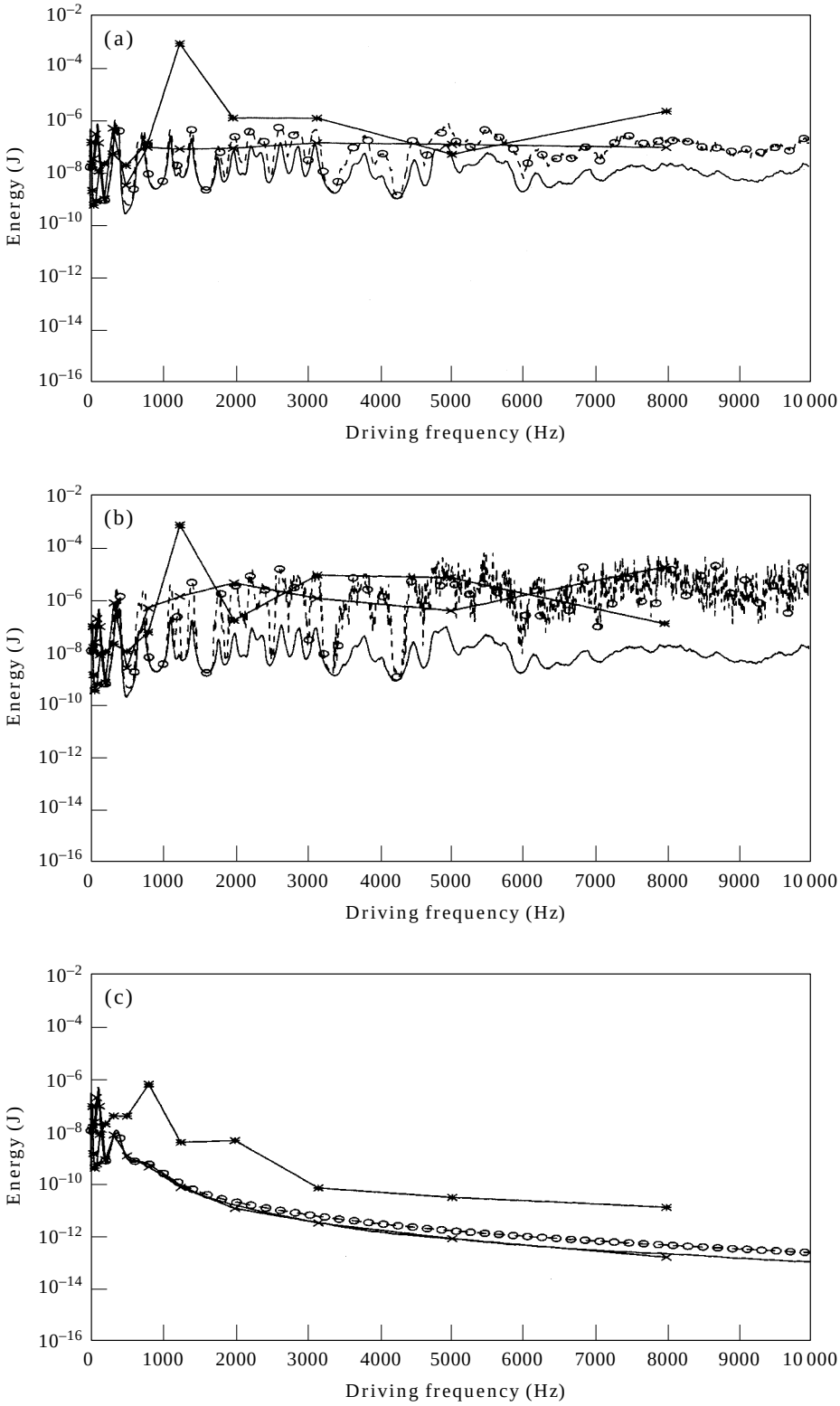
(a)
(b)
(c)
Energy (J)
10^{-2}
10^{-4}
10^{-6}
10^{-8}
10^{-10}
10^{-12}
10^{-14}
10^{-16}
0 1000 2000 3000 4000 5000 6000 7000 8000 9000 10 000
Driving frequency (Hz)

Figure 15(a–c)

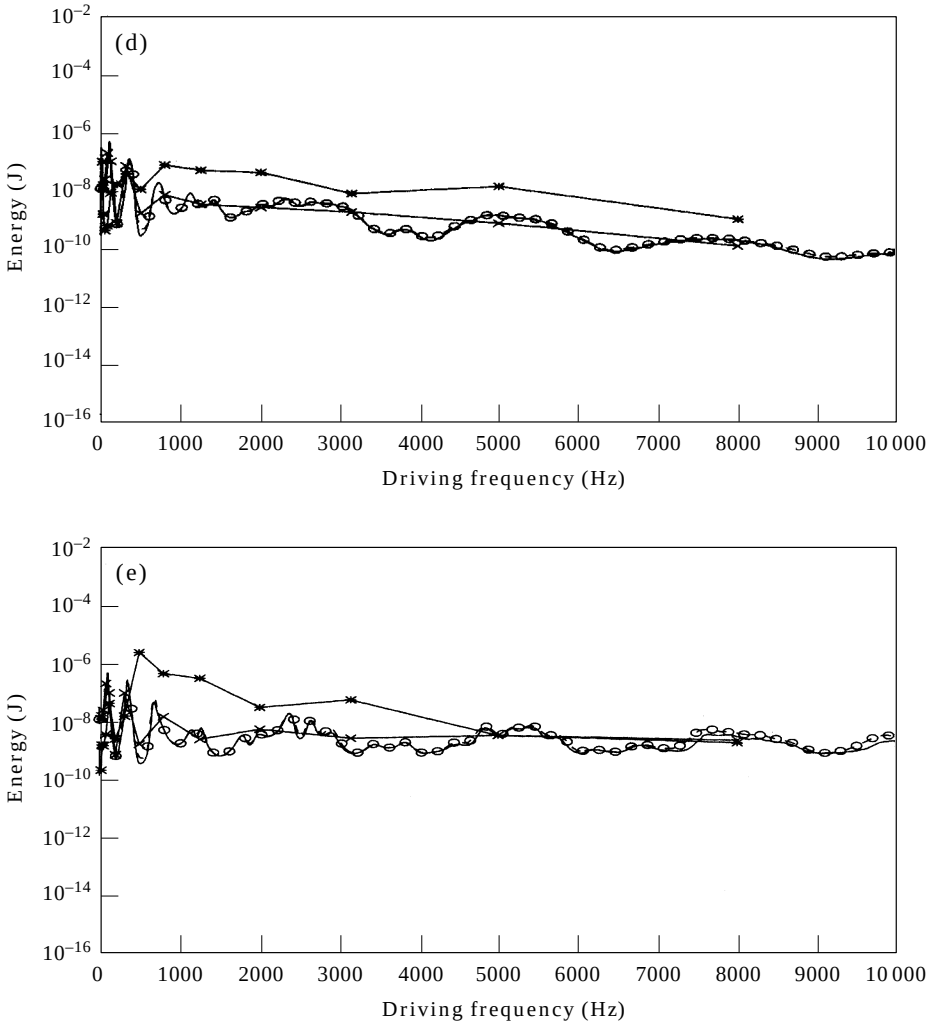

Figure 15. Comparison of ensemble averages and SEA results for member 3; -○-○-, ensemble mean; —, 50 percentage point; -×- × -, SEA: method I; -*-*-, SEA: method II. (a) Damping type (a); (b) damping type (b); (c) damping type (c); (d) damping type (d); (e) damping type (e).

to validate the ergodicity assumptions underlying the frequency band averaging of the energy spectra.

8. CONCLUSIONS

This study reports on numerical experiments conducted on statistics of vibration energy flow characteristics in randomly parametered lattice structures. The direct dynamic stiffness matrix method and Monte Carlo simulation procedures have been used in this study. The vibration analysis of sample problems is exact and, within the framework of accuracy of Monte Carlo simulation procedures, the statistical treatment of the problem is also exact. Particular attention is paid to

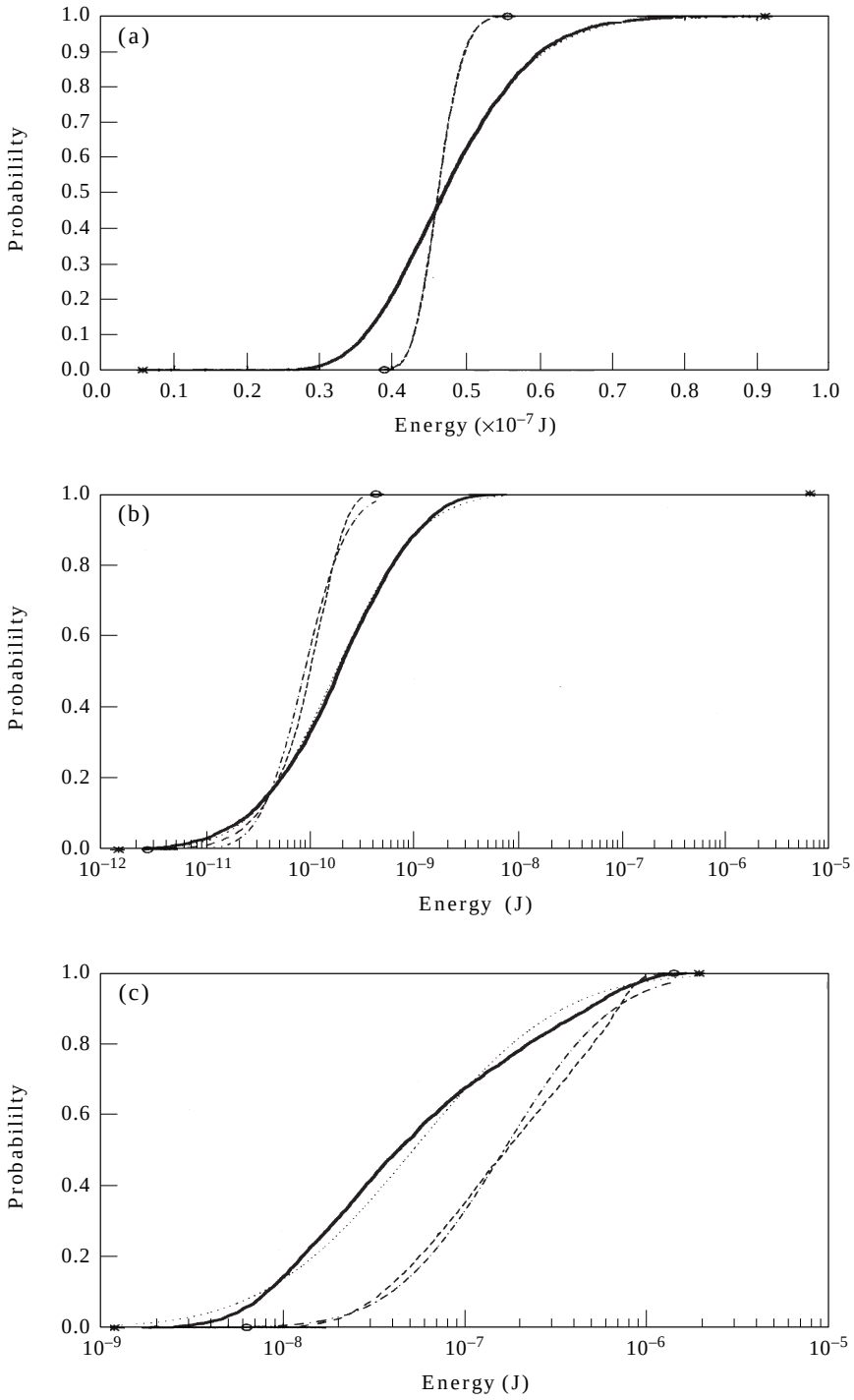

Figure 16. Probability distribution function of $E(\omega)$ for member 3; damping type (a); —, uncertainty model A, simulation; . . . . . , uncertainty model A, empirical; - - , uncertainty model B, simulation; - . .- . .- , uncertainty model B, empirical; *, extreme values, uncertainty model A; ○, extreme values, uncertainty model B. (a) Driving frequency = 80 Hz; (b) driving frequency = 500 Hz; (c) driving frequency = 2000 Hz.

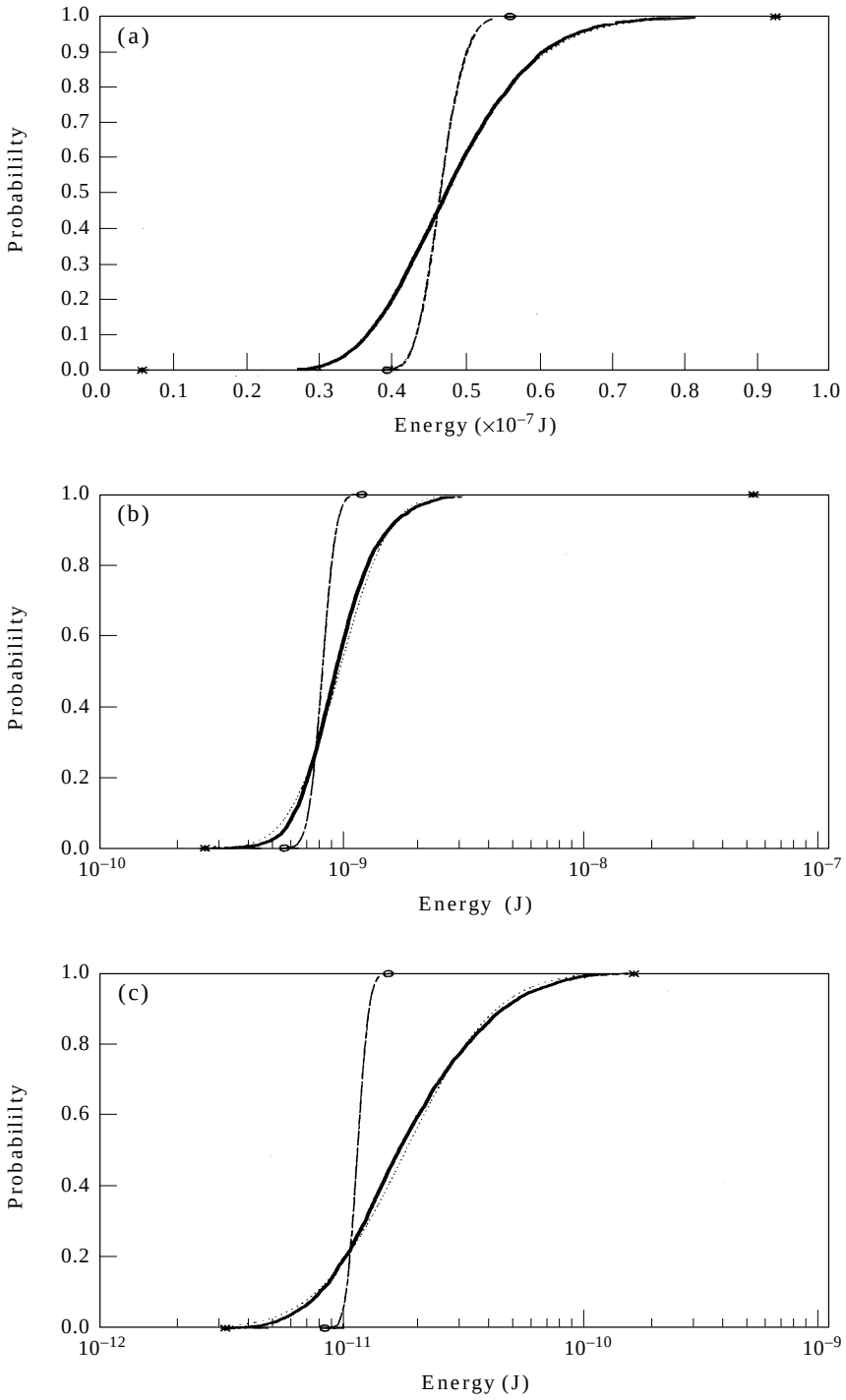

Figure 17. Probability distribution function of $E(\omega)$ for member 3; damping type (c); —, uncertainty model A, simulation; . . . . . , uncertainty model A, empirical; - - , uncertainty model B, simulation; - . .- . .- , uncertainty model B, empirical; *, extreme values, uncertainty model A; ○, extreme values, uncertainty model B. (a) Driving frequency = 80 Hz; (b) driving frequency = 500 Hz; (c) driving frequency = 2000 Hz.

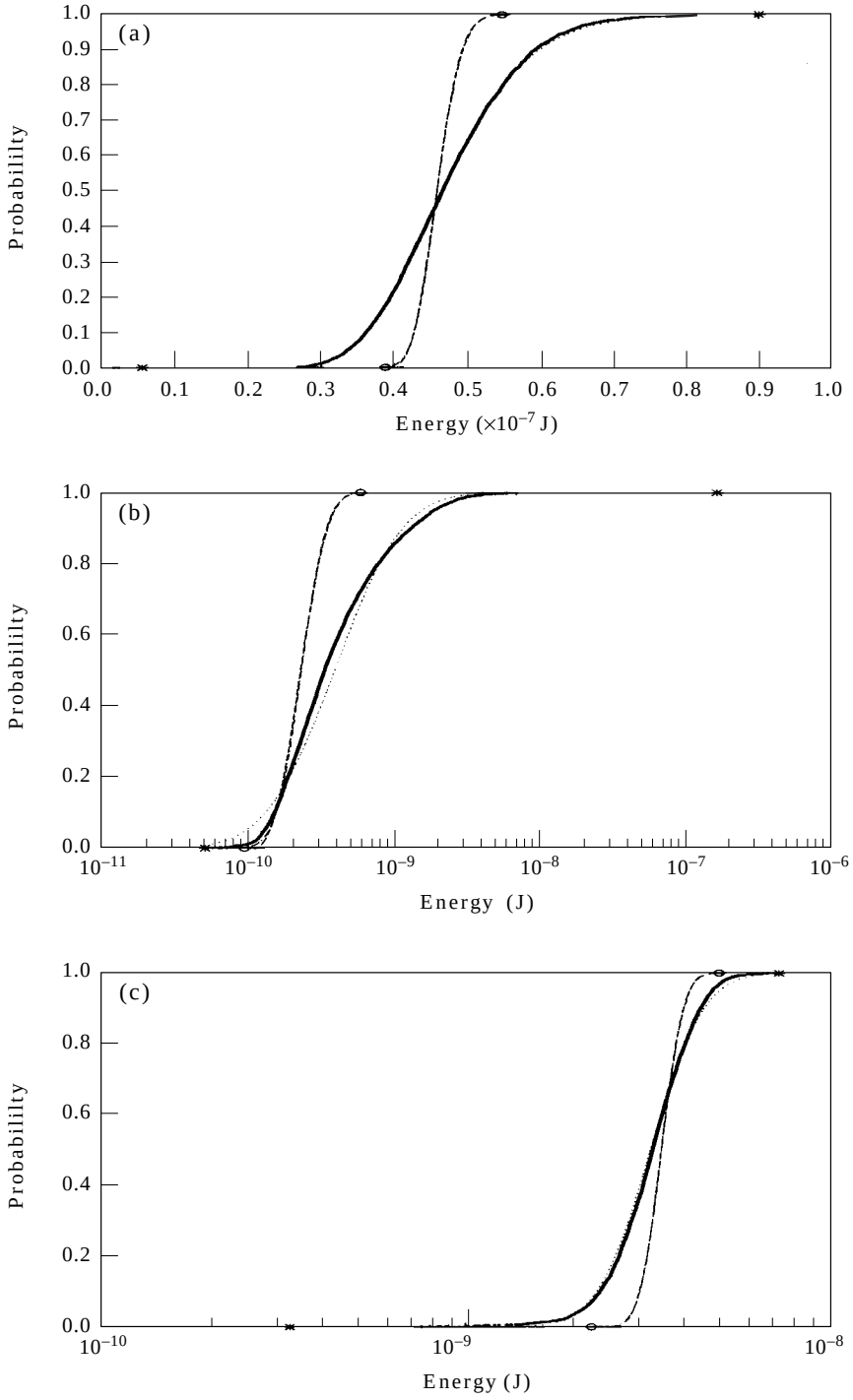

Figure 18. Probability distribution function of $E(\omega)$ for member 3; damping type (e); —, uncertainty model A, simulation; . . . . . , uncertainty model A, empirical; - - , uncertainty model B, simulation; - . .- . .- , uncertainty model B, empirical; *, extreme values, uncertainty model A; ○, extreme values, uncertainty model B. (a) Driving frequency = 80 Hz; (b) driving frequency = 500 Hz; (c) driving frequency = 2000 Hz.

the role played by different damping models and uncertainties associated with structure geometry. Comparisons of the ensemble averages with results from SEA formalisms involving frequency band averages are also made.

The following conclusions emerge from this study: (1) When the subsystems have strain rate viscous/hysteretic damping, the mean response prediction by SEA is likely to yield satisfactory results with the confidence bands narrowing on to the mean for increasing frequencies. For subsystems with velocity dependent viscous/hysteretic damping, the confidence bands, even for large driving frequencies, do not converge on to the mean. (2) Uncertainties arising from truss geometry affect the vibration energy variability significantly. (3) The energy spectra are non-Gaussian in nature. In the majority of cases, lognormal probability distribution was found to fit the energy spectra data well over a wide range of system parameters. This fit was obtained with the knowledge of the mean and standard deviation of the energy spectra. Thus, not withstanding the fact that the energy spectra are non-Gaussian distributed, knowledge of the mean and standard deviation enables the prediction of 5% and 95% probability points with reasonable accuracy. (4) SEA results based on frequency band averages and which take into account the "far" coupling effects, produce mean results which compare well with the ensemble mean. The estimation of standard deviation by frequency band averaging does not produce acceptable results. Accordingly, it would follow that the problem of confidence band estimation in SEA is intractable within the framework of frequency band averaging over a single realization of energy spectra.

ACKNOWLEDGMENT

The work reported in this study has been supported by funding from the Department of Science and Technology, Government of India.

REFERENCES

1. C. H. Hodges and J. Woodhouse 1986 *Reports on Progress in Physics* **49**, 107–170. Theories of noise and vibration transmission in complex structures.
2. R. S. Langley 1989 *Journal of Sound and Vibration* **135**, 499–508. A general derivation of the statistical energy analysis equations for coupled dynamic systems.
3. A. J. Keane 1992 *Proceedings of Royal Society of London* **A436** 537–568. Energy flows between arbitrary configurations of conservatively coupled multimodal elastic subsystems.
4. F. J. Fahy 1994 *Philosophical Transactions of Royal Society of London* **A346**, 431–447. Statistical energy analysis: a critical overview.
5. R. H. Lyon and R. G. DeJong 1995 *Theory and Application of Statistical Energy Analysis*. Boston MA: Butterworth-Heinemann; 2nd edition.
6. A. J. Keane and W. G. Price (editors) 1997 *Statistical Energy Analysis*: *An Overview with Applications in Structural Dynamics*. Cambridge: Cambridge University Press.
7. H. G. Davies and M. A. Wahab 1981 *Journal of Sound and Vibration* **77**, 311–321. Ensemble averages of power flow in randomly excited coupled beams.
8. H. G. Davies and S. I. Khandoker 1982 *Journal of Sound and Vibration* **84**, 557–562. Random point excitation of coupled beams.

9. F. J. Fahy and A. D. Mohammed 1992 *Journal of Sound and Vibration* **158** 45–67. A study of uncertainty in applications of SEA to coupled beam and plate systems, part I: computational experiments.
10. A. J. Keane and C. S. Manohar 1993 *Journal of Sound and Vibration* **168**, 253–284. Power flow variability in a pair of coupled stochastic rods.
11. C. S. Manohar and A. J. Keane 1993 *Journal of Sound and Vibration* **165**, 341–359. Axial vibrations of a stochastic rods.
12. C. S. Manohar and A. J. Keane 1994 *Philosophical Transactions of Royal Society of London* **A346**, 525–542. Statistics of energy flows in one dimensional subsystems.
13. A. J. Keane 1996 *Journal of Sound and Vibration* **192**, 139–158. Vibrational energy flows between coupled membranes.
14. E. Rebillard and J. L. Guyader 1995 *Journal of Sound Vibration* **188**, 435–454. Vibrational behavior of a population of coupled plates: hyper sensitivity to the connection angle.
15. B. R. Mace 1992 *Journal of Sound and Vibration* **154**, 321–341. The statistics of power flow between two continuous one-dimensional subsystems.
16. E. C. N. Wester and B. R. Mace 1996 *Journal of Sound and Vibration* **193**, 793–822. Statistical energy analysis of two edge-coupled rectangular plates: ensemble averages.
17. M. Paz 1984 *Structural Dynamics*. New Dehli: CBS Publishers.
18. R. S. Langley 1990 *Journal of Sound and Vibration* **141**, 207–219. A derivation of the coupling loss factors used in statistical energy analysis.
19. K. Shankar and A. J. Keane 1995 *Journal of Sound and Vibration* **181**, 801–838. A study of the vibrational energies ot two coupled beams by finite element and Green function (receptance) methods.
20. C. S. Manohar and S. Adhikari 1998 *Probabilistic Engineering Mechanics* bf **13**, 39–52. Dynamic stiffness of randomly parametered beams.
21. S. Adhikari and C. S. Manohar 1998 *International Journal of Numerical Methods in Engineering*, Accepted for publication. Dynamical analysis of framed structures with statistical uncertainties.
22. A. J. Keane and W. G. Price 1987 *Journal of Sound and Vibration* **117**, 363–386. Statistical energy analysis of strongly coupled systems.
23. S. A. Hambric 1990 *Journal of Vibration and Acoustics*, *Transactions of ASME* **112**, 542–549. Power flow and mechanical intensity calculations in structural finite element analysis.
24. C. Simmons 1991 *Journal of Sound and Vibration* **144**, 215–227. Structure-borne sound transmission through plate junctions and estimates of SEA coupling loss factors using the finite element method.
25. K. Shankar and A. J. Keane 1997 *Journal of Sound and Vibration*, **201,** 491–513. Vibrational energy flow analysis using a substructure approach: the application of receptance theory to FEA and SEA.
26. F. F. Yap and J. Woodhouse 1996 *Journal of Sound and Vibration* **197**, 351–371. Investigation of damping effects on statistical energy analysis of coupled structures.
27. D. A. Bies and S. Hamid 1980 *Journal of Sound and Vibration* **70**, 187–204. *In situ* determination of loss and coupling loss factors by the power injection method.
28. B. L. Clarkson and M. F. Ranky 1984 *Journal of Sound and Vibration* **94**, 249–261. On the measurement of the coupling loss factor of structural connections.